NBSIR 83-2643

Wave Form Simulations for Josephson Junction Circuits Used for Noise Thermometry

U.S. DEPARTMENT OF COMMERCE
National Bureau of Standards
National Engineering Laboratory
Center for Applied Mathematics
Washington, DC 20234

January 1983

U.S. DEPARTMENT OF COMMERCE
NATIONAL BUREAU OF STANDARDS

NBSIR 83-2643

WAVE FORM SIMULATIONS FOR JOSEPHSON JUNCTION CIRCUITS USED FOR NOISE THERMOMETRY

F. Sullivan, D. Kahaner, H.A. Fowler,
and J. Knapp-Cordes

U.S. DEPARTMENT OF COMMERCE
National Bureau of Standards
National Engineering Laboratory
Center for Applied Mathematics
Washington, DC 20234

January 1983

U.S. DEPARTMENT OF COMMERCE, Malcolm Baldrige, *Secretary*
NATIONAL BUREAU OF STANDARDS, Ernest Ambler, *Director*

WAVE FORM SIMULATIONS FOR JOSEPHSON JUNCTION CIRCUITS USED FOR NOISE THERMOMETRY

F. Sullivan, D. Kahaner, H.A. Fowler, and J. Knapp-Cordes
Center for Applied Mathematics
National Bureau of Standards

INDEX

ABSTRACT

Solutions to the Resistively Shunted Junction (RSJ) Equation:

$$\beta\ddot{\phi} + (1 + \gamma\cos\phi)\dot{\phi} + \sin\phi = \alpha + k\omega\sin\omega t$$

for small β (= .001) have been approximated using the SDRIVE integration package. Various graphic displays are used to examine the output, including plots of ϕ, $d\phi/dt$, and $\sin\phi$ as functions of time; Poincare diagrams; and plots of the Lienard coordinate

$$z = \beta\dot{\phi} + \phi + \gamma\sin\phi$$

which has a close connection with the "slow manifold", as a function of ϕ, of $\sin\phi$, and of time. Integration is performed by separation of the second-order equation into a coupled pair of first-order equations, and numerically integrating with respect to time.

Several cases have been examined, for $\gamma < 1$, representing quiet behavior of resistively shunted thermometer oscillator devices. The report is an archive record of program-test data.

A case of "jump"(voltage-spike) oscillator performance for $\gamma = 1.5$ has been simulated in considerable detail, principally as a test of the integrator. Parallel, independent computer results (Sanders and van Veldhuizen, Amsterdam) were available for comparison. This case is of considerable mathematical interest, and values of $|\gamma|>1$ may also occur in the RSQUID thermometer.

INTRODUCTION

We are interested in numerical approximations to the solutions of the non-linear equation

$$\beta \ddot{\phi} + (1+\gamma \cos\phi)\dot{\phi} + \sin \phi = \alpha + k\omega \sin \omega t \quad ,$$

which is a model for simulating the behavior of the circuit consisting of a series connection of an inductor, a resistor and a Josephson junction (used as a noise thermometer). Here the variable ϕ is the time-dependent quantum-mechanical phase difference across the Josephson barrier, and the parameters represent combinations of circuit parameters, as well as the amplitude and frequency of the applied signal. We concentrate on the conditions of small β as is the case for the noise thermometer.

The value of the parameter γ is crucial to the behavior of solutions. If $|\gamma|<1$, we have the so-called "quiet" case. Taking $|\gamma|>1$ gives "jump" behavior. We will examine this dichotomy in more detail later, but for the

present consider the following: If $|\gamma|<1$, the coefficient of $\dot{\phi}$ is always positive and, hence, acts as a damping force. However, for $|\gamma|>1$ this term changes sign (at $\cos^{-1}(-\frac{1}{\gamma})$) and switches from damping to forcing. This causes rapid "jumps" in the wave form. Physically, the system develops short, high-amplitude pulses in its voltage output.

For the quiet case $|\gamma|<1$, β small and $\alpha>1$, intuition about the general solution can be gained by looking at the reduced first-order autonomous equation

$$(1+\gamma \cos\phi)\,\dot{\phi} = \alpha - \sin\phi$$

$$\phi(o) = \phi_o$$

This is integrated directly for t as a function of ϕ , giving a periodic motion with period

$$T_o = \frac{2\pi}{\sqrt{\alpha^2-1}}$$

The next step is to generalize to the first order driven equation for $\omega > 1$

$$(1+\gamma \cos\phi)\dot{\phi} + \sin \phi = \alpha + k\omega \sin \omega t \quad .$$

Using non-linear variation of parameters, averaging, and letting $\gamma \to 0$, Sanders [11] shows that there is a (winding) solution with period

$$T = \frac{2\pi}{\sqrt{\alpha^2 - J_o^2(k)}}$$

so long as $\left| \frac{\alpha}{J_o(k)} \right| > 1$. Here J_o is the zero order Bessel function. The Bessel

function behavior is borne out by experimental observation. Our numerical simulations show that the above is a good estimate of the period in the second order case, so long as β is small. The simulation also gives additional detailed information about the wave form, which is quite smooth for $|\gamma|<|$.

In case $|\gamma|>1$ the situation is very different. In order to see why, first notice that defining

$$z = \beta\dot{\phi} + (\phi + \gamma \sin\phi)$$

gives the Lienard co-ordinate formulation

$$\dot{z} = \alpha - \sin\phi + k\omega \sin \omega t$$

$$\beta\dot{\phi} = z - (\phi+\gamma \sin\phi) .$$

The curve $z = \phi + \gamma\sin\phi$ in the $\phi - z$ plane is called the slow manifold, [33] because $\dot{\phi} = 0$ on this curve. If we take ϕ modulo 2π, the curve has critical points at the two values of $\cos^{-1}(-\frac{1}{\gamma})$ and an inflection point at $\phi = \pi$.

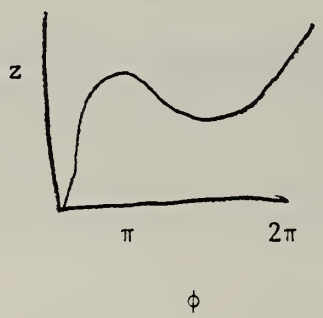

Suppose now that $\alpha>1$, and that we choose initial values of ϕ and z on the slow manifold (say at (0,0)). The "average" value of z over one cycle is positive, so that z tends to increase. However, for points (ϕ,z) above the slow manifold, $\dot{\phi}$ is positive while for points below $\dot{\phi}$ is negative. Hence, solution trajectories tend to be attracted to the slow manifold and move slowly up it until the first critical point is reached. On this part of the trajectory $d\phi/dz$ behaves approximately like

$$\frac{\dot{\phi}}{\dot{z}} = \frac{(z - (\phi+\gamma \sin))/\beta}{\beta\ddot{\phi} + (1+\gamma \cos\phi)\dot{\phi}}$$

$$= \frac{z - (\phi+\gamma \sin \varphi)}{\beta^2\ddot{\phi} + \beta(1+\gamma \cos)\dot{\phi}}$$

Since β is small, the denominator is close to zero, and for (z,φ) above the slow manifold $d\phi/dz$ becomes large. The solution "jumps" across to the other branch of the slow manifold. (This description can be made rigorous). The form which the jump takes depends very strongly on the initial conditions. It

is even possible for the solution trajectory to reach the critical point and loop back to the first branch before jumping across to the second branch.

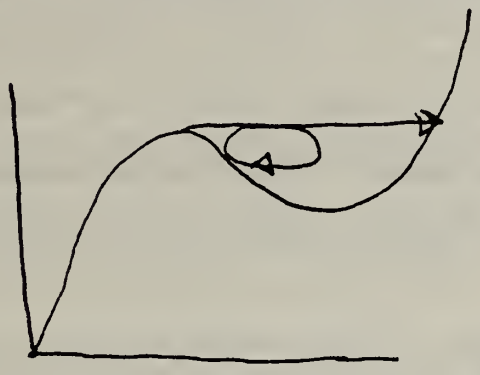

The time-dependent behavior of the wave-form in this situation can be seen in Figs. 23-37 below.

Using an asymptotic expansion, Sanders [11] obtains expressions for the time at which the jump occurs. If k=0 (the autonomous second order equation), and γ is close to 1, the period of the solution is approximated by $T = To + \Delta T$

where $$T_o = \frac{2\pi}{\sqrt{\alpha^2-1}} \quad \text{and} \quad \Delta T = \frac{9}{2} \frac{(1-\gamma)^2}{\alpha^2} \cdot$$

In two driven cases which we have examined, with larger values of γ-1 (γ= 0.5 and γ = 1.5), this formula yields too large a value for the observed ΔT; the time-averaged limit cycle is better approximated by the Bessel-function expression mentioned above.

HISTORICAL SYNOPSIS

The second-order RSJ* equation, in autonomous form, was proposed by McCumber [1] and Stewart [2] on the basis of the Josephson relations:

$$V(t) = \partial\phi/\partial t \cdot h/2e \qquad I_{sc}(t) = I_c \sin\phi$$

combined with Kirchoff's laws for the circuit in which the tunneling element is connected. (Here V and I_{sc} are, respectively, the voltage across and the supercurrent through the tunneling barrier; ϕ is the superconducting-phase difference; and I_c, the critical current). Their objective was to explain the (time-averaged) dc current-voltage characteristic curve which they observed for the circuit.

Kamper [3], and Kamper and Zimmerman [4] have suggested that a point contact (the Josephson junction) facing an inductive loop in series with a very low resistor might serve as a unique form of noise thermometer. Soulen and Giffard [5] applied the RSJ model to describe the behavior of the circuit in which the Bessel function dependence was derived. A recent paper by Gallop [6] surveys the importance of Josephson SQUID noise thermometry, as an absolute temperature calibration standard.

Peterson, Soulen, and Van Vechten [7],[8],[9] examined a first-order-accuracy solution to the time-dependent driven equation. (A recent manuscript by Sanders [11] clarifies the same picture for second order.) This provides a partial description of the frequency perturbations in the relaxation oscillation observed when the drive amplitude is varied. In addition to the relaxation frequency dependence on drive amplitude, through a Bessel function expression (which is expected from the model, and observed experimentally), a weak upward or downward slope is found experimentally. This may be simulated partially by expanding the Bessel-function solution to the first-degree equation, and partially by the inclusion of interactions with the (external) tank circuit. Puzzling problems remain such as the observed occurrence of "doubled" peaks; R. Soulen, Private Comm., [11A] and it is clear that neglect of the second derivative leaves the treatment incomplete.

Schlup (1979) [10] has offered a relatively complete model for behavior of the small-beta autonomous case. The treatment by Sanders [11] links the autonomous relaxation oscillation to a Hopf bifurcation from the solutions on the zero-voltage step (that is, when the bias-current term alpha has values below one.)

Driven Case for beta large

The case of beta large ($\beta \gg 1$) has recently been rather broadly treated. Schlup (1974) [12] provided a numerical solution for the time dependence, in this the near-Hamiltonian-oscillator case. His paper was the first to include specific effects from the γ term. Belykh, Soerensen, and Petersen I and II [13,14] have provided a survey of possible solutions for the autonomous and driven cases, respectively.

*The abbreviation RSJ (Resistively Shunted Junction) equation is in common use for this equation, which may variously appear without the $\beta\,\phi$, $\gamma\cos\phi$, or $k\,\omega\sin\omega t$ terms. The term R-SQUID noise thermometer refers to the circuit described above.

Connections of the case $\gamma = 0$ and $\beta > 1$ with bifurcations, chaos, and oscillator instability have been examined by Packard, Huberman, et al. [15,16,17]; in detail by R. Kautz, [18,19,20], and by Pederson and Davidson [21], who looked at amplifier stability over a broad range of frequency and amplitude parameters. This case has important applications to phase-locked frequency-to-dc-voltage converters, and to microwave parametric amplifiers.

Driven case for beta small, and gamma non-zero.

The detailed parametric treatment of the RSQUID* noise thermometer has been begun by Soulen, Park, Seppa, and Van Vechten [22,23,24] . Careful estimates of realistic parameter ranges have been made by Van Vechten [25].

Extremely fast transitions between parts of the slow manifold appear at once if gamma is assumed larger than one. These render the solution of the first degree equation at best an unsatisfactory approximation to the full wave form. Cushman [26] has completed a global treatment of existence of periodic solutions for the second-order autonomous equation, based upon a general model of flows in phase space. Important results from this case include indications of the strong global stability of solutions in the autonomous case, for all values of gamma; and rapid convergence of these to the periodic solution.

Sanders [11] has offered an approach to the "jump" ($\gamma > 1$) cases, which is inspired by the work of Levi [28], and which proceeds from recent successful treatments of the van der Pol equation by Grasman and collaborators [29,30]. These techniques, in turn, are based upon Smale's work in differential topology.

On the basis of this wide spectrum of interest in the mathematical features of the driven (forced) equation, and its physical consequences as a simulation, we have been led to an approach which stresses detailed, accurate numerical integration combined with varied graphics displays.

RSQUID = Resistor - Superconductive Quantum Interference Device

THE ALGORITHM

The numerical procedure for integration has been to separate the second-order equation into two coupled first-order equations:

$$\dot{Y1} = Y2 / \beta$$

$$(1) \qquad \dot{Y2} = -(1 + \gamma \cos Y1)\cdot Y2 / \beta + \alpha - \sin Y1 + k\omega \sin \omega t$$

$$\text{so that} \qquad Y1 = \phi \qquad \dot{Y1} = \dot{\phi}$$

$$Y2 = \beta\dot{\phi} \qquad \dot{Y2} = \beta\ddot{\phi}$$

This is not a unique separation. Another choice for Lienard coordinates comes from noticing that

$$\beta\ddot{\phi} + (1 + \gamma\cos\phi)\dot{\phi} \quad , \text{ is an exact differential.}$$

In that case

$$\text{let} \qquad z = \beta\dot{\phi} + (\phi + \gamma\sin\phi) \quad , \text{ so that}$$

$$(2) \qquad \dot{z} = \alpha - \sin\phi + k\omega \sin\omega t$$

$$\text{and} \qquad \beta\dot{\phi} = z - (\phi + \gamma \sin\phi)$$

Although the first choice of Lienard coordinates appears to involve more multiplications, this choice is numerically more stable than the second because β is small and z stays close to $(\phi+\gamma\sin\phi)$. However, the second pair has some independent mathematical interest, as has been mentioned.

Integration is performed by using either SDRIV3 in single precision or DDRIV3 in double precision [35]. These programs utilize implicit multistep integration formulas, either of Gear or Adams Moulton, to track the solution components of (1) or (2) to within certain specified local error criteria. The nonlinear algebraic equations which result can be solved by any of several algorithms, including Newton's method, in which case the Jacobian of the system can be given explicitly or computed numerically. Various output options are also available.

STRUCTURE OF THE PROGRAM

The main program, CUSHEQ/DOUBLE, simulates the operation of the physical system by querying for parameters and initial value settings, through the subroutine OQUERY/DOUBLE; driving the DDRIVE integrator with its attached F1 (Non-autonomous terms) and JACOBN (Jacobian) subroutines; returning values at time intervals of $\frac{S\cdot 2\pi}{\omega}$ where S is an input real number; and storing the values of t, Y1, Y2 in arrays.

These values are written to a file by the subroutine OPRINT/DOUBLE and may later be graphed in a variety of ways through the program SPREAD/DOUBLE, which offers nine options of two-dimensional plotting. SPREAD collects the values of ϕ and $\dot{\phi}$, and evaluates sin ϕ and z (to single precision) in one loop.

This functional structure of the subroutines is illustrated in Table I.

INPUT INSTRUCTIONS

The operator is queried for input values of

A = α

B = β

C = γ

D = δ = 1 (a parameter coefficient of the sin ϕ term, which is kept in reserve for later approximations)

E = $k\omega$

W = ω, the circular frequency of the drive term, scaled to $\omega_c = \frac{2e}{\hbar} RI_c$ *

S, a real number, which selects the time intervals of $\Delta t = \frac{S \cdot 2\pi}{\omega}$ at which numerical results will be returned from the integrator; and for initial choices of

$$Y1 = \phi$$

$$Y2 = \dot{\phi}$$

$$T = t$$

TOL = the numerical tolerance for the completed integration. Finally, the number N (= number of points to be returned) is requested.

* See Appendix B for the circuit.

TABLE I

SUBROUTINE STRUCTURE OF THE PROGRAM CUSHEQ

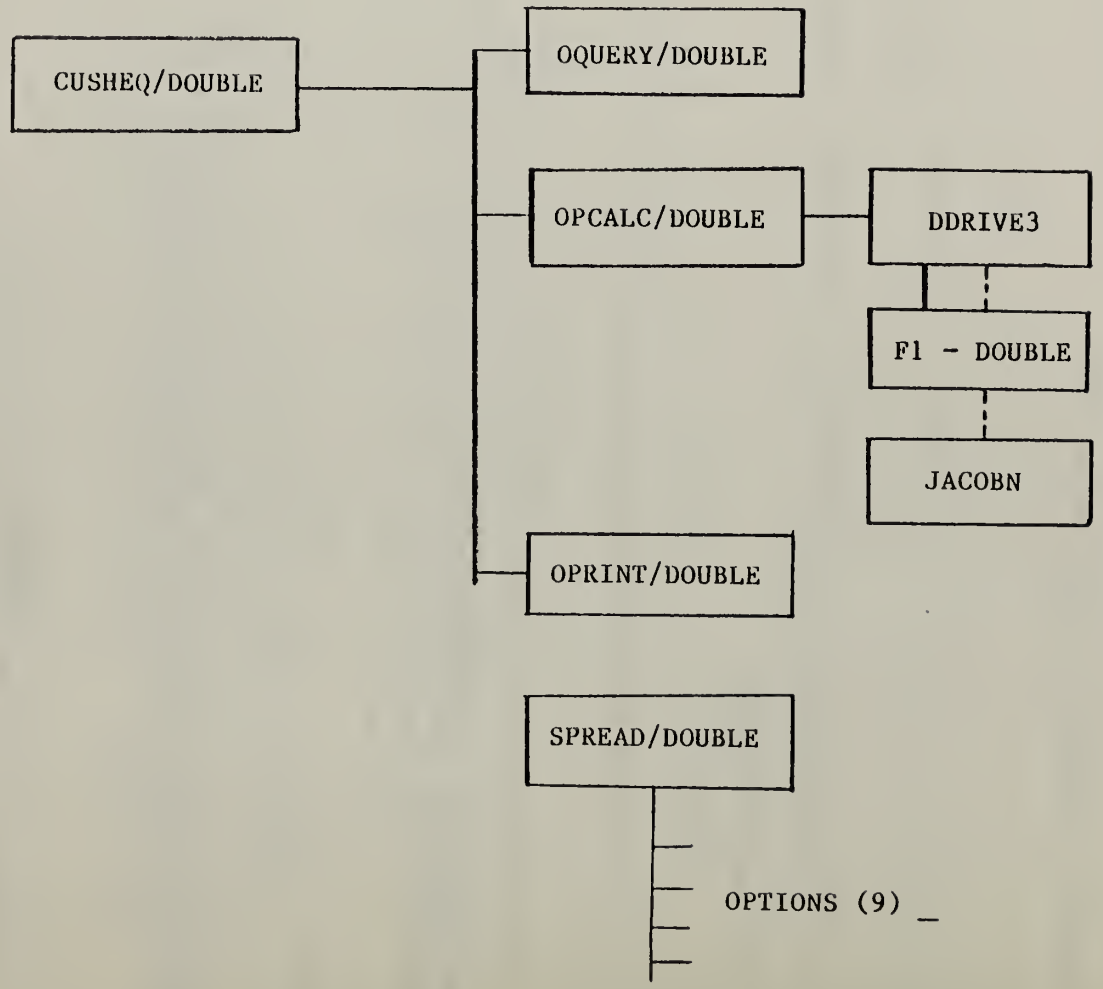

GRAPHICS OUTPUT CHOICES

The graphics output subroutines can be combined with appropriate choices of S to produce a very large variety of displays. These will only be briefly described; they are best illustrated through examples of use.

Option (1): The Poincare map routine, of $\dot{\phi}$ vs ϕ mod 2π , is conventionally used in non-linear analysis to distinguish fixed points, stable and non-stable orbits, etc. In the present case, selection of S permits the time interval to be taken as the period of the drive oscillation (S = 1), or any multiple or fraction thereof.

Option (2): As mentioned on p. 9 , z is constructed by SPREAD from the stored values of Y_1 and Y_2. The plot of ϕ vs z is useful in distinguishing transition phenomena for the high-speed "jump" intervals which occur for the choices of gamma larger than 1, where the term $\gamma \cos \phi$ can have negative values greater than 1.

Option (3): ϕ vs t is the actual time-dependent solution of the equation, simulating the barrier-phase-difference for the Josephson effect. ϕ is plotted mod 2π, since otherwise the secular term in its solution would cause it to "ramp" off the page.

$\dot{\phi}$ vs t simulates the instantaneous time-dependence of the barrier voltage.

Option (4): The return map of $\dot{\phi}$ at intervals corresponding to the drive period is a method of exploring both the subharmonic structure of the solutions, and the jumps between branches of the slow manifold which the system may exhibit.

Option (5): sin ϕ vs t simulates the instantaneous flow of supercurrent through the barrier of the Josephson junction. There are a number of interesting insights and visual simplifications introduced by the cylinder projection of viewing which the sine function provides. The physical quantity ϕ is not an observable; it represents the argument of a trignometric function which is an observable, and ϕ can, therefore, be thought of as confined to motion on a cylinder.

Option (6): sin ϕ vs z and

Option (7): z vs sin Φ illustrate the same effects as Option (2), but in cylindrical projection, relating z to the (observable) supercurrent.

Option (8): z vs t collects the values of ϕ and $\dot{\phi}$ as returned by the main integration, and calculates z , displaying it as a function of time. The smoothness of this function, when its individual terms are undergoing rapid derivative changes with repect to time, is a measure of the performance of the program as a whole.

Option (9): ϕ/t vs t provides a mechanism for averaging the advance rate of the quantum-mechanical phase difference, a measure of the relaxation, or limit frequency

$$\langle\dot{\phi}\rangle = \lim_{T\to\infty} \frac{1}{T} \int_0^T \dot{\phi}(t)dt$$

It is calculated by computing Y1/t values from the output array, while suppressing the mod 2π reduction used in plotting ϕ , in option (3) above.

SCALING OF THE EQUATION TO THE PHYSICAL PROBLEM

Time Scaling

Drive and relaxation frequencies are scaled to the real physical parameters of the thermometer oscillator circuit through the "equivalent plasma frequency"

$$2\pi\ \omega_c = \frac{2e}{h} RI_c \qquad \text{in circular measure , or}$$

$$\nu_c = \frac{2e}{h} RI_c \qquad \text{in direct frequency measure (Hz)}$$

The quantity $\frac{2e}{h}$ is known extremely accurately, from voltage stabilization experiments, to have a value of 483.6 MHz/microvolt *.

and for $R = 10^{-5}$ ohms (the shunt resistor-see Appendix B) with $I_c = 10^{-6}$ amps

$$\nu_c = (483.6 \times 10^{12}) \times 10^{-5} \times 10^{-6} \quad \text{Hz}$$

$$\nu_c = 4.836 \times 10^3 \text{ Hz} \quad \text{or } 4.836 \text{ kHz} \quad \text{, specifically when the}$$

product RI_c is equal to 10^{-11} volts.

Selected Drive Frequencies

A value for ω of 200, scaled to the circuit parameters above, corresponds to

$$200 \times 4.836 \times 10^3 = 967 \text{ kHz}$$

Or, a value for ω of 800 corresponds to 3.869 Mhz.

And, a value for ω of 45.68 is equivalent to

$$45.68 \times 4.836 \times 10^3 = 220.9 \text{ kHz}$$

These are the values of drive frequency used in the simulations reported below.

---

* From high-precision experiments against the U.S. standard volt cells, this quantity is known at better than one part per million accuracy. The rounded version to four decimal figures is used here, for computational simplicity.

Time-dependent quantities

Time-dependent quantities in the RSJ equation are expressed in voltage units for simulation purposes:

thus $\alpha = 1$ for $R\ I_c = 10^{-11}$ volts-dc, in the examples used, and therefore $k\omega = 1$ corresponds to an rf input signal at 10^{-11} volts-rf amplitude (not rms).

Output $\dot{\phi} = Y_2/\beta = 1$ has the scale (10^{-8} volts) and $\sin \phi = 1$ corresponds to $I_{sc} = I_c = 10^{-6}$ amps.

The parameter β

Soulen [7] estimates a value of the second-derivative coefficient β at .001, as reasonable for point contact RSQUID devices. We note that a capacitative value of β as small as .01 has been suggested for experiments on tunnel junctions, by Fulton [34]. This does not provide strong guidance for the case of point contacts, however, because of the different physical barrier-layer present. The value .001 is consistent with the curves of Fig 2 and Fig. 5 in McCumber [1]. We select beta positive to assure that the second derivative term will have a limiting effect during the " jump" intervals for cases of γ greater than one.

Beta vs omega plane

If we consider the plot of beta versus reduced frequency ω/ω_c which is found in Kautz [19] as Fig. 2 of that article, the value $\beta = .001$ in conjunction with the line where

$$\omega L = 1/\omega C \quad \text{, its resulting value}$$

$$\beta^{-1/2} = 31.62$$

would lie along the lower edge of region VI extended to the upper left. in Kautz's log-log beta-omega plane. Since the values chosen for ω/ω_c, namely 200, 800, and 45.68, are above this, our simulations lie up in the region between that lower-edge value and the line where $R = 1/\omega C$

$$\beta^{-1} = 1000$$

This is equivalent to saying that our results have been limited to a frequency region above the junction/circuit "equivalent" plasma frequency. Such information is helpful when comparing behavior between different families of Josephson oscillators.

Choice of γ

γ from theory is proportional to $I_c L_e$, where I_c is of the order of 10^{-6} amps and L_e, the inductance of the coupling loop which the Josephson junction faces, is estimated to be about 2×10^{-10} henries.

If we take the expression derived by Peterson[8] for gamma in the RSQUID circuit:

$$\gamma = \frac{2\pi}{h} \cdot 2e \times L_e I_c = 2\pi \times \frac{2e}{h} \times L_e I_c$$
$$= 2\pi \times 483.6 \times 10^{12} \times 2\times10^{-10} \times 10^{-6} = 0.6077$$

for the above values. Here we see that $L_e > 0.33$ nanohenry will suffice to render $\gamma > 1$. γ, as shown by Soulen, Peterson, and Van Vechten [7] can be adjusted experimentally to fall either below or above 1. It is a parameter which can be determined in a coarse manner within the experiment. Of particular interest are the cases in the transition region as γ approaches 1 from below. In some cases there are anomalies in the observed relaxation frequency as a function of drive amplitude. Previous work has not shown whether all of these result from an intrinsic wave form of the relaxation oscillator, or from its coupling to the drive and detection circuits.

A. Tests of Quiet Cases with Smooth Wave Forms

Simulation of the quiet thermometer oscillator has proceeded by examining several cases for $\gamma < 1$. These results can be compared with existing asymptotic models (Soulen [5,7]; Sanders [11]) and directly with experiment. The graphics routines have been used to simulate the waveforms in considerable detail.

The curves which follow in Figs. 1-10 correspond to the case $\gamma = 0.8$, $\omega = 200$, $\alpha = 0.5$, which corresponds to a drive frequency of 967 kHz and a relaxation frequency of about 25 kHz. Figs. 11-15 are run with the drive frequency four times as large; i.e. 3.869 MHz.

Figs. 1-5 — "Test 30"
Parameters:
A = 5, B = .001, C = 0.8, D = 1.0, E = 382, S = .025, T = 0, TOL = 10^{-8}, W = 200, 3000 points

This is a fairly low drive amplitude, simulating a waveform which is primarily the relaxation oscillation, modulating a "carrier" wave at the drive frequency.

Fig. 1 shows phi, the solution, as a function of elapsed time t. The fine-grain vertical oscillations are at the drive, or "carrier" frequency; the broad stripes conform to the relaxation or limit cycle of the Josephson oscillator.

The points on Figs. 1, 2, 3 have been returned by the program at the rate of one per 1/40 of the drive cycle. The numerical values have been generated at double precision (parts in 10^8). Phi is plotted modulo 2π, to prevent the plot from ramping diagonally off the paper.

Fig. 2 shows the time derivative of phi, simulating the instantaneous Josephson voltage across the tunneling barrier. Note that this appears to be primarily amplitude-modulated by the relaxation oscillation, but that the positive peaks in the envelope are slightly offset in time from the negative ones. The mean value of phidot is expected to approximate A, or α ; the time offset is a consequence of the value of C, or γ .

Fig. 3 shows the sine of phi, simulating the instantaneous supercurrent through the barrier. This is equivalent to taking the function of Fig. 1 and wrapping it around a cylinder, whose axis proceeds along the time direction. The resulting "wrapped ribbon" is viewed from the side; note that the zero at the bottom of Fig. 1 has now been displaced to the center of Fig. 3. Note that the ribbon returns down the "far"side of the cylinder with steeper slope than it rises on the "near" side. A time-smoothed version of the instantaneous supercurrent would appear to be primarily amplitude-modulated at the relaxation frequency; Fig. 3 suggests that this would be a somewhat asymetric sawtooth as a function of time, with a slow rise and a more rapid return to the negative limit of -1.

Fig.4 shows z versus phi for these points. 4b and 4c illustrate z vs. sin ϕ, to suggest the cylindrical projection which controls the actual values of the tunneling supercurrent. Fig. 5 shows the composite Poincare map.

Each point in these diagrams can be tracked to corresponding instantaneous values in Figs. 1,2,3. These methods of display are useful in examining periodicity and stability properties.

Figs. 6-10 — "Test 38"
Parameters:
Identical with "Test 30", except E=1402 , about 3.6 times as large. The waveforms become more frequency-modulated in character.

Fig. 6 shows phi as a function of time. Note that the fine-grain vertical oscillations have been replaced by stripes moving along the ribbon, and that some of these stripes appear to cross over each other. Note that the open bands which appeared before have now been eliminated; the ribbon runs together or overlaps on itself.

Fig. 7, corresponding to Fig. 2, now shows quite a different form of voltage signal. The maximum amplitude is nearly uniform, as in a frequency-modulated waveform. A sixth harmonic of the relaxation oscillation shows up. The offset of positive- from negative-peaks seen in Fig. 2 is now reflected in the interior "cluster" detail.

Fig. 8. The ribbon winding of Fig. 3 has been widened to the point that it overlaps itself. At the same time, the "carrier"-frequency detail is now somewhat suppressed, as we should expect if the sidebanding of frequency modulation is superimposed.

Figs. 9 and 10 correspond to Figs. 4 and 5. Some changes of form are observed.

Test of Higher Drive Frequency and "Demodulation"

Figs. 11-15 — "Test 61"

Parameters:
A = 5, B = .001, C = 0.8, D = 1.0, E = 1528 , S = 1.0, T = 0, TOL = 10^{-4} , W= 800, 3000 points

This is roughly similar to the conditions of Figs. 1-5, except that the drive frequency has been increased by a factor of four, and the amplitude of the drive signal increased to produce roughly the same level of amplitude of the "carrier". In addition, only one point is returned per cycle of the drive, instead of forty; thus, the drive signal disappears from view in the output. The horizontal time scale has been compressed by a factor of ten in plotting.

Fig. 11 shows phi as a function of elapsed time. The profile of the relaxation oscillation is the dominant detail. In electrical engineering terms, the "audio" signal has been mathematically "demodulated" from the "rf carrier" and its sidebands, and is displayed here by itself.

Fig. 12 shows instantaneous voltage. Here we are seeing a sort of stroboscopic view of one of the traces which can be seen extending through Fig. 2. It gives only a limited, partial view of the full waveform which would be experienced if we were seeing all phases of the "carrier" cycles.

Fig. 13 , a correspondingly "stroboscopic" view of the supercurrent could be correlated with one of the lengthwise threads along the ribbons in Fig. 4 or Fig. 8. Note that this is a continuous smooth path —but in Figs. 4 and 8 there may be crossing of these paths. Whether ribbon twisting can take place under the proper conditions on C and E (gamma and k omega) is an interesting problem relating to the frequency stability of the oscillator.

Figs. 14 and 15 are smooth curves, much as expected for a stable system.

Tests at a Low Value of $(\alpha - 1)$

We may select $\alpha = 1.2$ in order to emphasize the perturbations on the relaxation frequency which are caused by varying the amplitude of the drive term. At the same time, the selection of $\omega = 200$ simulates a drive frequency of 967 kHz, while the chosen value of alpha corresponds to a relaxation frequency of ~ 5.8 kHz. We now have quite a large band separation between the drive, or carrier frequency, and the relaxation or limit cycle frequency of the Josephson oscillator. Figs. 16-22 below are a simulation of this case.

The theory by Peterson, Soulen, and Giffard [5,8,9], which is based on consideration of the first-derivative term only, gives a value for this correction:

$$\omega_{rel} = \alpha\left(1 - \frac{J_0{}^2(k)}{\alpha^2}\right)^{1/2} \times \omega_c$$

A series of curves has been run for these values of alpha and omega, over a range of k from 1.91 to 8.65, which is designed to cover the first three zeros of the Bessel function. The relaxation frequencies, which may be read off to better than 1% from the plots, do follow the amplitude dependence predicted from this theory of the first-order equation. This corresponds to the period of the "winding" solution of Sanders, mentioned in the Introduction.

Figs. 16-18 — "Test 4"
Parameters:
A = 1.2 , B = .001, C = 0.5, D = 1.0 , E = 730, S = 0.20 , T = 0 , TOL = 10^{-4}
W = 200; 3000 points.

There are five points returned per drive cycle.

Here we expect fully quiet, smooth oscillator behavior. Because of the low value of alpha, different paths occur for the off-set "strobe" positions around the drive cycle. This is particularly clear in the "wrapped-cylinder" paths of Fig. 18.

We note parenthetically that the projection of Fig. 18 is taking the sine of a phi-function which already comprises several low harmonics of the "fundamental" relaxation frequency. "Sine of sines" implies a Bessel-function set of harmonic coefficients. In this case, the argument of the Bessel functions is the drive amplitude. Therefore in Fig. 18 it is not surprising that we find patterns suggestive of very simple Fourier-component mixes, in various relative time phases.

The patterns seen in Figs. 17 and 18 bear close qualitative resemblances to the experimentally "demodulated" audio spectrum of an actual thermometer, when the first six or eight harmonics of the relaxation frequency are allowed to pass the audio filter.

Figs. 19-21 — "Test 7"
Parameters are the same as in Figs. 16-18 above, except that the drive amplitude is now increased to 1730, i.e. 2.37 times as large.

At this particular amplitude the fundamental Fourier coefficient $J_1(k)$ must be at a high value. Also, the paths overlap from one relaxation cycle onto the next, which is only slightly the case in test 4 above.

Fig. 22 illustrates the perturbation of the Josephson relaxation frequency by the amplitude of the drive signal, which is one of the key problems in physical variation, for which an answer is sought.

The crosses are estimated numerical values of the relaxation frequency scaled to the critical frequency w_c , obtained from the 2π - crossings of phi vs t , in the series of which Figs. 16 and 19 are examples. Scatter of these points is about 6 parts in 10^3; it comes partly from numerical roundoff of the single-precision integration, and partly from interpolation errors in estimating the 2π crossing points.

The circles are points taken by interpolating between curves of Peterson [8, esp. Fig. 2), which is actually calculated for $\alpha = 1.25$, rather than $\alpha = 1.2$, the value for which Figs. 16, 19 ... have been run. Note that the curves in Peterson's article are plotted on a squared scale; here we show frequencies directly. The curve described by the circles has been normalized to the first two maxima in the crosses — this scale is shown at the right.

We conclude from this comparison that the positions vs k of the first two maxima and minima, and the magnitude of the swings between, show agreement within the available limits of error. In broader terms, the second-order simulation appears to be agreeing in detail with the predictions of the first-order model, which in turn are known to model a portion of the observed experimental behavior.

B. Tests of "Jump" Case($\gamma = 1.5$) with Discontinuous Waveform Derivatives

The case of gamma larger than one can occur in R-SQUID noise thermometers. This comes about by increasing the pressure on the Josephson point contact, so that the critical current I_c increases, for the same value of exterior L_e into which the junction faces; gamma is proportional to the product of I_c and L_e.

The first-derivative term in the equation causes rapid transitions when $(1 + \gamma \cos \varphi)$ changes sign. These rapid transitions, on a greatly compressed time scale, give a very rigorous test of the integrator. While $\cos \varphi$ is negative,

$\dot{\varphi}$ rises or falls very quickly to an extreme value, then turns around and returns quickly until the solution is "caught" again as the $\gamma \cos \varphi$ term reaches -1 , and the system reverts to a "slow manifold" solution.

The problem of "jumps" of this type has already been studied for the case of the Van der Pol oscillator [29,30] "Drops" and "slices" occur, as presented by Littlewood [31,32]. Our approach has been primarily through graphics techniques, using the integrator program to simulate the physical evolution of

the system as nearly as possible. We have simulated a description through the "slow manifold" approach, which was suggested by Cushman [33]. We have had available to us a set of independent calculations by Sanders and Van Veldhuizen, [27] using a different Shampine-Gordon integrator, which confirm critical details of the program performance, especially for these "jump" details.

The parameter values are chosen as follows:

$$\beta = .001 \ , \ \gamma = 1.50 \ , \ k = 1.0 \ , \ \alpha = 11.0 \ \ \omega = 45.6800 \ , \ k\omega = 45.6800$$

S has been chosen in a variety of ways, to display different details.

This simulates a Josephson thermometer with shunt resistor value $R = 10^{-5}$ ohms, with critical current $I_c = 10^{-6}$ amps, driven at 220.9 KHz and at a drive amplitude k = 1.0, which places its operation in the "very weakly driven" part of the Bessel-function plot for relaxation frequency (below the first maximum). We note that this choice of parameters has the following special features, which are <u>not</u> common to the best operating thermometer devices: very low drive, or carrier amplitude; drive frequency near the fourth harmonic of the Josephson relaxation oscillation frequency, which appears to lead to phase locking between the two oscillations, and sharp voltage "spiking" associated with the negative-resistance intervals when $(1+\gamma\cos\phi)$ is negative.

Thus, a value for ω of 45.68 for this choice of R and I_c would correspond to

$$45.68 \ \times \ 4.836 \ = 220.9 \text{ kHz}$$

the observed average relaxation frequency is 101/421 of that value; this corresponds roughly to the ratio between $\alpha = 11$ and $\omega = 45.68$.

There is, however, a perturbation associated with the amplitude factor k for the drive term. The theory by Peterson, Soulen, and Giffard gives a value for this correction to the predicted relaxation frequency

$$(1 - J_o^2/(11)^2)^{1/2} \ ,$$

where the argument of the Bessel function $J_o(k)$ is 1 in the case we have chosen. The corrected, predicted relaxation frequency would then be 53.0651 kHz; we find in simulation the value 52.9970. The reason for this discrepancy of 0.13% is not clear — the observed value is lower than the predicted.

<u>Results of the Integration</u>

When started from $\phi = 0$, $d\phi/dt = 0$, a point which is off the stable trajectory, the solution evolves quasi-periodically for about 1000 drive cycles, then settles into the stable periodicity, reproducing itself to about 2 parts in 10^5, in both ϕ and $d\phi/dt$. It is not clear whether failure to cycle more closely than this represents a fluctuation associated with phase locking, in the physical system. Both exact and approximated Jacobian routines have been tried at varying levels of precision, with similar results.

We find the numerical solution, in double precision, to be multiply periodic, with a prominent subharmonic at 421 times the drive period $2\pi/\omega$, and at 101 times the relaxation period. This determines the average relaxation frequency, from the repetition rate, to be $101/421 \times 45.6800$ very precisely (to the order of parts in 10^5). There is a family of nearly-periodic structures appearing ; "quasi-subharmonics"(?) reflected in the patterns of modulation of the high-frequency spikes in $d\phi/dt$.

It is not clear at this early stage of the analysis, whether this rational subharmonic relation is a consequence of frequency-locking of the relaxation oscillation, via subharmonics, to the nearest subharmonic of the drive frequency. We note that for the parameters chosen, the drive frequency is a little more than four times the relaxation frequency, and hence " band separation" is incomplete. Also, the observed relaxation frequency is offset towards a lower value than that suggested by the simple theory, e.g., there may be a "pulling" of the relaxation frequency by the frequency locking.

Operation of the program at single precision, in other parameter ranges, indicates that the spikes originate with the increase of γ to about one; when γ reaches a value about 1, at this drive amplitude, the spikes may be negative in sign as well as positive; at 1.5 they can occur in multiples as well as singly.

Fig. 23 ϕ , the superconducting phase-difference across the tunneling device, is shown modulo 2π as a function of time. Note that on the up-going transitions between steps, in the relaxation oscillation, only a relatively few points are caught in the ϕ transition region near π . The function is a continuous staircase moving upward off the plot.

Fig. 24 $\dot{\phi}$, the instantaneous voltage, is shown on a very much reduced scale. There are sharp positive-and negative-going excursions (to positive 800 and to negative 600) during the very brief time intervals when ϕ is near π. Other plots indicate that its mean value lies around 4 to 5 on the stable manifold points. Evidently the spikes contribute a substantial part of the mean voltage $\approx$ 10 or 11.

Fig. 25 $\sin\phi$, the instantaneous current in the junction loop, is displayed for the same points. Roughly, it appears as a sinusoid at the drive frequency, added to a linear ramp from the relaxation oscillation. (Note that this ramp is not derived from the numerical "chopping", modulo 2π , of Fig.1, and is smoothly continuous across those drops); the drops in Fig. 25 represent quite drastic reversals of the supercurrent direction through the junction, including some "extra" reversals going to the current limits, associated with the large spikes in the plot of the instantaneous voltage. In the case of the Josephson point contact facing into an inductance, the phenomena represent pulses of supercurrent sharpened by the inductance. Closer examination reveals that Fig. 25 actually "wraps" Fig. 23 around a cylinder, with the "jump" regions of very rapid current reversal occurring on the " far" side, as viewed in projection.

Figs. 26 and 27 $z = \beta \dot{\phi} + \phi + \gamma \sin \phi$ the coordinate which was suggested as an alternative separation variable, is shown plotted against ϕ, for 2 sets of points taken at time intervals corresponding to π/ω and $0.1\ \pi/\omega$ from the time zero of the sin ωt driving term, respectively. (a modified type of Poincare plot). Two branches of the slow manifold are seen; the points corresponding to π/ω wobble upward on the left-hand branch to the maximum, then jump across the central "unstable" zone. The points corresponding to $0.1\ \pi/\omega$ .... wobble downward on the right-hand branch, then jump across to the left [with a lower minimum slope than the up-going jump points].

Figs. 28, 29, 30 and 31 display the same data as a function of sin ϕ. We note that ϕ appears to be a cyclic function of z, modulo 2π; however we can only conclude from this that it is a continuous function of z.

Figs. 28 and 29 are representative of fully stabilized cycles in the solution. Figs. 30, 31, and 32 are data which include the early transient behavior as the system is started from (0,0) at t=0.

Fig. 33 which shows z as a function of t, should be compared against Fig. 23 and 25. It will be noted that the drops in Fig. 33 are only those associated with the arithmetic operation of reducing ϕ to values modulo 2π. z in this plot is simply the sum of terms phi, phidot, and sin ϕ, evaluated from the

returned ϕ and $\dot{\phi}$ of the integrator program, with ϕ expressed modulo 2π.

z as a function of t evolves smoothly as a linear ramp, with an added sinusoid at the "carrier" frequency. The slope of the ramp reflects the relaxation frequency. This smooth evolution takes place through the " jump" discontinuities in the time derivatives of the other functions plotted; its behavior confirms the general internal consistency of those solutions.

Thus z vs t is like Fig. 23 in portraying the continous evolution of a "rotating" solution; however, its rate is uniform, and does not exhibit the cycle of the relaxation oscillation.

Long-Time Behavior

Figs. 34 and 35 illustrate Long-time or Very Slow Behavior

If the results illustrated in Fig. 3 and Fig. 5 are extended by plotting only one point per drive cycle, and greatly compressing the time scale (3000 drive cycles, or about 12 milliseconds, is the duration of the plot shown here) the result is an interesting "stroboscopic imaging" of the long-term motion. After the first 1000 drive cycles, the motion is fully periodic and the diagram repeats itself to parts in 10^5.

The upward "return tracks" record the intervals at which extreme values of voltage spikes recur (the subharmonic 421/101).

Fig. 35 is the same type of plot, but calculated with $\gamma = 0.5$ instead of 1.5. The "stroboscopic path" is greatly smoothed, and more nearly sinusoidal. In this case, voltage "spiking" is not present. The maximum value of phidot encountered in this run is about 14.

Careful examination of this diagram reveals that the pattern at the right hand end is starting to repeat, after time = 330.4 on the time scale of the plot. Examination of printout shows that this doubly-periodic solution is reproducing itself to within 3 or 4 parts in 10^4.

The repetition period corresponds to 2402 drive cycles, or 577 periods of the relaxation oscillation. The high rational "winding ratio" may be used to estimate the numerical value of the relaxation period, averaged over the long repetition period and expressed in units of $2\pi/w$.

$$\tilde{T}_{rel} = \frac{2402}{577} = 4.16291$$

For comparison, the "autonomous" relaxation period expressed in the same units

$$\underline{w} = \frac{45.680}{11.0} = 4.1527273$$

when corrected by the Gifford-Soulen-Peterson-Sanders factor

$$\frac{\alpha}{\sqrt{\alpha^2 - J_o^2(k)}} = (.9975775)^{-1}$$

for $\alpha = 11$ $k = 1$ yields the value 4.16281.

We conclude from this that the "autonomous" relaxation period, corrected by this Bessel-function formula, agrees accurately with the average relaxation period seen in the simulated solution of the second-order equation, for $\gamma = 0.5$.

Figs. 36 and 37 show confirmation between a result from Sanders, on a problem of critical variation, and the same answer as calculated by this program. For this test the frequency w is set at 45.68128 (slightly different from the values used in the preceding series of figures), and the initial value of ϕ is varied in steps of less than 2 parts in 10^7.

The initial value of phi is chosen as follows:

a) 6.374423
b) 6.374424
c) 6.374425
d) 6.374426
e) 6.374427
f) 6.374428

This variation produces changes of the order of 1 in the output waveform (phi versus time), which is that corresponding to a triple crossing of the region where $1 + \gamma \cos \phi < o$.

In Fig. 37 the horizontal lines represent the values of ϕ for which $1 + \gamma \cos\phi$ vanishes.

Summary of Observations

These tests of quiet and "jump" cases have produced a variety of graphical and numerical output. We summarize here a few of the more interesting results.

Quiet cases

- For $\gamma < 1$ (at least as high as 0.8) all waveforms are smooth, regardless of the amplitude of the drive signal. There is a gradual transition resembling that from amplitude-to frequency-modulation, as the drive amplitude is increased.

- A useful memory device is to think of ϕ as an argument function confined to move on a cylinder. Sin ϕ , the instantaneous supercurrent, is then visualized as a projection on a plane parallel to the axis of the cylinder.

- A type of mathematical "demodulation" or separation of the low-frequency relaxation oscillation from the high-frequency "carrier" is easily achieved by making the return interval of the integrator program coincide with the period of the drive signal.

- Tests at a low value of $(\alpha-1)$ give good agreement with the Bessel-function dependence of relaxation frequency (period) on drive amplitude coefficient k .

"Jump" case

- As expected from first-order theory, the simulation exhibits "jumps" between parts of the slow manifold. These rapid transitions can be accurately traced out in full detail, provided by the second-order equation. They are accompanied by sharp voltage pulses.

- The solution is observed to be doubly periodic at high precision, with the relaxation oscillation at the 421/101 subharmonic of the drive frequency. Since the drive signal has been selected near the 4th harmonic of the relaxation frequency, we suspect that phase-locking is occurring because of the strong overlap between the "audio" and "carrier" bands. Thus it may be difficult to compare the observed repetition period of the relaxation, with a theoretical prediction based solely upon values of α, k , and γ . Unlike the quiet cases which were considered above, the solution may have a relaxation frequency which wanders from a constant value during the "long" 421 repetition period, while averaging to a mean value which is frequency-locked to the drive frequency.

- Plots of z versus phi exhibit sharp details of the "up-going" and "down-going" transitions between parts of the slow manifold. If phi is shown in cylindrical projection, the connection with current reversals going to the critical limits can be made clear.

- Plots of z versus time exhibit the uniform advance of a smooth function, apparently sinusoidal at the drive frequency, atop a highly linear ramp; this in spite of the fact that its three constituent terms show discontinuities in their derivatives. This suggests the possibility of further simplifications, in pursuit of a numerically simple routine for evaluating relaxation period (frequency).

Conclusions as to the Accuracy of the Integrator

- Figs. 36 and 37 demonstrate the independence of the solution method from details of algorithm, programming, and machine; and also the high sensitivity of both NBS's and Sanders' algorithms to critical changes in initial conditions. The figures are an illustration of how small changes in the initial conditions can generate dramatic changes in the behavior of the wave form as $\phi(t)$ traverses the region where $1+\gamma \cos \phi < 0$. This is an instance of the changes from 'dips' to 'slices' which were studied by Littlewood for the case of the van der Pol equation.

  A tolerance of 10^{-10} is needed to produce Figs. 36 and 37. Accumulation of error is a well known phenomenon in numerical solution of o.d.e.'s. The accumulation of error eventually gives a completely wrong answer. An accumulated error of one part in 10^5 would alter the traversal of the $1+\gamma \cos \phi < 0$ region (as can be seen in Figures 36 and 37).

- The system is not "stiff". Considerations of accuracy restrict the step size. We obtained the most efficient integrations by using the Adams Moulton integrator coupled with Newton's method for the nonlinear equations. However, given sufficient machine precision any competent modern integration will correctly follow these solutions. This was confirmed by Sanders, et al, who obtained some similar results using entirely different software.

- The observed doubly-periodic cycling of the "jump" case for gamma = 1.5 is followed to parts in 10^5 for the observed output values of phi and phidot, after an initial "settling" period of about 1000 drive cycles. We associate this "settling" period with the approach of an "off-manifold" solution to the asymptotically stable form.

- The results just mentioned were obtained only at double-precision 10^{-8} tolerance requirement. Improving the tolerance to parts in 10^{10} did not produce distinguishable improvements. By contrast, single precision (parts in 10^4) produced "time-slippage" which threw off the accuracy of the long-time-period cycling. Although general features of the single-precision runs were similar to the double-precision ones, they clearly lacked the full detail and accuracy. (We note that errors in phi and phidot are cumulative with time, so that an error of one part in 10^8 per cycle can accumulate to one part in 10^5 after 1000 cycles).

  These results are in accord with expectations, since the double-precision integrator is expected to perform distinctly better in the rapid transitions between the "slow manifold" and the "jump" intervals.

  For the "quiet" cases where gamma is less than 1, the distinction in behavior between single- and double-precision routines is expected to be less sharp, since they do not have to adjust to the "jump" transitions.

CONTINUING DIRECTIONS OF THE INVESTIGATION

- With the reliability of the integrator now confirmed by severe tests, we wish to apply it to some major unsolved problems of the experiments. One such is the behavior of

$$\langle\dot{\phi}\rangle = \lim_{T\to\infty} \frac{1}{T} \int_0^T \dot{\phi}(t)dt$$

  vs k for a driven $\gamma>1$ case. Sanders [11] gives an estimate of the period $T_o+\Delta T$ for a $\gamma>1$ autonomous case, and the formula

$$T = \frac{2\pi w}{\sqrt{\alpha^2 - J_o^2(k)}}$$

  for a $\gamma<1$ driven case.

  We are trying to learn more about the observed anomalous "doubling" in the driven $\gamma>1$ case. We had to have an utterly reliable integrator before attempting this.

  Foremost in interest will be to run with a wide range of drive amplitude values, up to k = 8 or 9, for values of gamma between 1 and 2; the output quantity of interest will be phi divided by $t-t_o$, evaluated to a part in 10^4, for comparability with the experimental observations, which have shown examples of "doubling" at the parts-in-10^3 level, not in accord with a simple Bessel expression.

- Return-mapping techniques will be tried, in order to examine questions of frequency stability, especially the possibility of chaotic behavior. Chaotic, or erratic behavior of the observed relaxation frequency would be expected to interfere with the desired high-fidelity operation of the Josephson thermometer as a voltage-to frequency converter of thermal (Nyquist) noise.

- An asymptotic expansion formula derived by Sanders [11] may provide a key to developing Fourier analysis of the "quiet" waveforms, such as Figs. 16-21. This will be explored in further detail.

- The programs will be rendered transportable (with consideration being given to its possible future use on smaller machines than the Univac 1100/82). Jill Novotny is currently installing it on the Catholic University DEC 10.

ACKNOWLEDGMENTS

We wish to record the contributions of numerous colleagues.

R. Soulen and D. Van Vechten of the Temperature Standards Division, NBS formulated the RSJ equation in the present context, to analyze their experimental results. Soulen, Van Vechten, and R. Peterson (of the Electro-magnetic Technology Division, NBS Boulder) developed first-order-accurate solutions for the equation in first order. R. Rehm and H. Baum, of Mathematical Analysis Division and Center for Fire Research, NBS, suggested a two-timing approach to the solution of the first-order equation, by a singular-perturbation expansion.

A. Deprit of Mathematical Analysis Division, recognizing the similarity between this equation and the Van der Pol oscillator, proposed to R.H. Cushman (of Rijksuniversiteit Utrecht and a guest worker in Mathematical Analysis Division) that some classical techniques of nonlinear dynamics be tried on the problem. Cushman has developed a global theory for the phase flow of the autonomous second-order equation. This has led to the important suggestion that the Lienard coordinate z be used to examine the stability effects of the driven equation. Cushman outlined the problem to Jan Sanders (Vrije Universiteit, Amsterdam), who has proceeded independently with an asymptotic analysis. In conjunction with van Veldhuizen (Mathematisch Centrum, Amsterdam) Sanders has developed an integrator and a mapping approach to the unstable cases. We are indebted to Sanders for permitting us to see his computations and his Ms. on asymptotics, before publication. Sanders's outline for the asymptotics is consistent with the earlier proposal by Rehm.

Richard Kautz (Electromagnetic Technology Division, NBS Boulder) has published two papers treating the parameter space for the large-beta case. Using a Runge-Kutta integrator, he has examined bifurcations and chaos for the driven oscillator in the large-beta (quasi-harmonic-oscillator) case. These papers convinced us of the usefulness of an approach through a capable integrator routine.

R. Henry of the Physics Department, Bucknell University, has provided us with a pre-publication copy of a manuscript on mapping technique, applied to the frequency stability of voltage-controlled oscillators. This provides very important insights, using a simple and powerful approach.

Subsidized computer time on the NBS UNIVAC 1100/82 system has been generously supported by the National Engineering Laboratory and the Center for Applied Mathematics, as a portion of their Competence development budget for FY 1982.

We are indebted to Jill Novotny for running out many of the plots which are exhibited here, and for composing a compact User's Guide for the CUSHEQ/DOUBLE program.

BIBLIOGRAPHY WITH NOTES

This listing omits many basic references to the methods of nonlinear dynamics, which are utilized in the solution techniques which have been followed.

It includes only the sources for Josephson-effect devices and theory which seem to us to be most directly pertinent to the problem at hand. Since 1963 there is a very large literature of Josephson devices in other applications. Closely related to the problem of the second-degree RSJ equation is the Sine-Gordon equation with damping term; a literature has proliferated on the "fluxon" or "kink" solutions to that equation. The Sine-Gordon equation is the partial differential equation which is appropriate for a Josephson junction which is space-distributed: i.e. it is being operated at a high enough frequency that its surface area must be considered to have parts which are out of synchronism with each other.

The Josephson name is attached to (1) the basic electrodynamic relations of the superconducting tunneling effects; (2) several differential equations which have been attached to these problems; (3) some other unrelated problems in very-low temperature phase changes. Readers encountering titles in this field for the first time should be careful which is meant.

1. D.E. McCumber, Effect of ac Impedance on dc Voltage-Current Char's of Supercond. Weak-link Junctions, J. Appl. Phys. 39, 7, 1968, pp.3113-18
    Develops the beta parameter for both capacitive and inductive loadings.
        Capacitance.

2. W.C. Stewart, Current-voltage Characteristics of Josephson Junctions, Appl. Phys. Letters 12, 8, 1968, pp.277-280
    Formulates RSJ Equation for autonomous case.
        Capacitance, Dissipation.

3. R.A. Kamper, Survey of Noise Thermometry, in Proc. 5th Symp. Temperature, Its Meas't & Control in Sci. & Ind., Washington, 1971, pp.

4. R.A. Kamper and J.E. Zimmerman, Noise Thermometry with the Josephson Effect, J. Appl. Phys. 42, 1971, pp.132-136

5. R.J. Soulen Jr. and R.P. Giffard, Impedance and Noise of an rf-biased RSQUID operated in the non-hysteretic regime, Appl. Phys. Lett. 32, 1978, pp.770
Discusses low-frequency variation of alpha causing thermometer frequency spectrum.

6. J.C. Gallop, The Impact of Superconducting Devices, Metrologia 18,2, 1982, pp.67-92 (esp. p. 86)
Discusses present temperature ranges and level of precision for Jos. thermometers.

7. D. van Vechten, R.J. Soulen, Jr., and R.L. Peterson, Behavior of the dc Impedance of an rf-biased resistive SQUID, in "SQUID '80", H.D. Hahlbohm and H. Lubbig. ed., Berlin (de Gruyter), 1980, pp.569-584
Presents examples of the most difficult unexplained experimental anomalies.

8. R.L. Peterson, Mathematical Modeling of the Impedance of a Resistive rf SQUID, J. Appl. Phys. 52, 12, 1981, pp.7321-26
Solution for average period in heavy dissipation, by a Bessel function expansion.
RSJ Equation, Electronic Experiment.

9. R.L. Peterson and D. Van Vechten, Modeling the Impedance of a Josephson-junction Noise Thermometer, Phys. Rev. B24, 6, 1981, pp.3588-91
DC Voltage approximated from period by a Bessel-function Expansion.
RSJ Equation, Experiment, Computer Simulation.

10. W.A. Schlup, Relaxation Oscillations of a Josephson Contact, ZAMP 30, 1979, pp.851-857
Autonomous equation is solved; limit cycles are examined in detail..

11. J. Sanders, The Josephson Equation; an Example of Asymptotics: MANUSCRIPT TO BE PUBLISHED, Springer Mathematics Lecture Notes Series, July 1982, pp.
Seen in hand-drafted form.

12. W.A. Schlup, I-V Characteristics & Stationary Dynamics of a JJ including Interference Term, J. Phys. C7, Solid State Physics, 1974, pp.736-748
Includes Cosine term; large beta microwave case; model includes normal-current flow.

13. V. Belykh, N. Pedersen and O.Soerensen, Shunted Josephson Junction Model I. The Autonomous Case., Phys. Rev. B16, 1977, pp.4853-59
A first extended treatment of parameter space.
RSJ Equation, Nonlinear Dynamics, Poincare Diagrams.

14. V. Belykh, N. Pedersen. and O. Soerensen, Shunted Josephson Junction Model II. The Non-autonomous Case., Phys. Rev. B16, 1977, pp.4860-71
Various Attractors are presented for parameter regions.
RSJ Equation, Nonlinear Dynamics, Poincare Diagrams.

15. N. Packard, Modelling Turbulent Phenomena, w. appl. to Josephson Junctions, Talk at NBS Temperature Division, 1981 (May 27).
Incl. Movie of Topological progression along Str. Attr.Manifolds.
Strange attractors, Topology, Mappings.

16. B.A. Huberman, J.P. Crutchfield, and N.H. Packard, Noise Phenomena in Josephson Junctions, Appl. Phys. Lett. 37, 8, 1980, pp.750-751.
Power vs. Frequency Bifurcation Diagram.
Noise, Strange attractors, Power Spectrum.

17. B.A. Huberman and A.B. Zisook, Power Spectra of Strange Attractors, Phys. Rev. Letters 46, 10, 1981, pp.626-628.
Shows integrated noise spectrum in the chaotic regime.
Noise, Strange attractors, Power spectrum.

18. R.L. Kautz, On a Proposed Josephson-effect Voltage Standard at Zero Current Bias, Appl. Phys. Lett. 36,5, 1980, pp.386-388.
Rationale and experiment for a stripline device.
Electronic Experiment, RSJ Equation, Stability.

19. R.L. Kautz, The AC Josephson Effect in Hysteretic Junctions: Range and Stability of Phase Lock, J. Appl. Phys. 52,5, 1981, pp.3528-41.
Numerical modeling of Weakly Dissipative RSJ Equation.
Stability, Bifurcations, Noise.

20. R.L. Kautz, Chaotic States of rf-biased Josephson Junctions, J. Appl. Phys. 52,10, 1981, pp.6241-46.
Full details of Bifurcation in Parameter Space.
Strange Attractors, Bifurcations, Spectral Analysis, Numerical Simulation.

21. N.F. Pederson and A. Davidson, Chaos and Noise Rise in Josephson Junctions, Appl. Phys. Lett. 39, 10, 1981, pp.830-832.
Frequency-Amplitude Parameter Plane for zero dc voltage, in amplifier applications.
RSJ Equation, Computer Simulation, Chaos, Stability.

22. G. Park, PRIVATE COMMUNICATION, Manuscript Notes, addressed to R. Soulen and D. Van Vechten, 1980.
Treats tank circuit of thermometer in interaction with the RSQUID loop.

23. H. Seppa and R.J. Soulen, Jr., Modeling the dc Impedance of an rf-driven R-SQUID, Post-deadline paper HY 15, American Physical Society Meeting, March, 1982.
Models resonance at tank-circuit frequency, by feedback around to the RSQUID loop.

24. R.J. Soulen, Jr., H. Seppa, and D. van Vechten, The Effect of Additive Noise & Bandpass Filters on the Performance of a JJ Noise Therm., Post-deadline Paper HY 15, American Physical Society Meeting, March, 1982.
Isolates and models a weak dependence on gain and on filter bandwidth.

FIG. 4

Z VS PHI

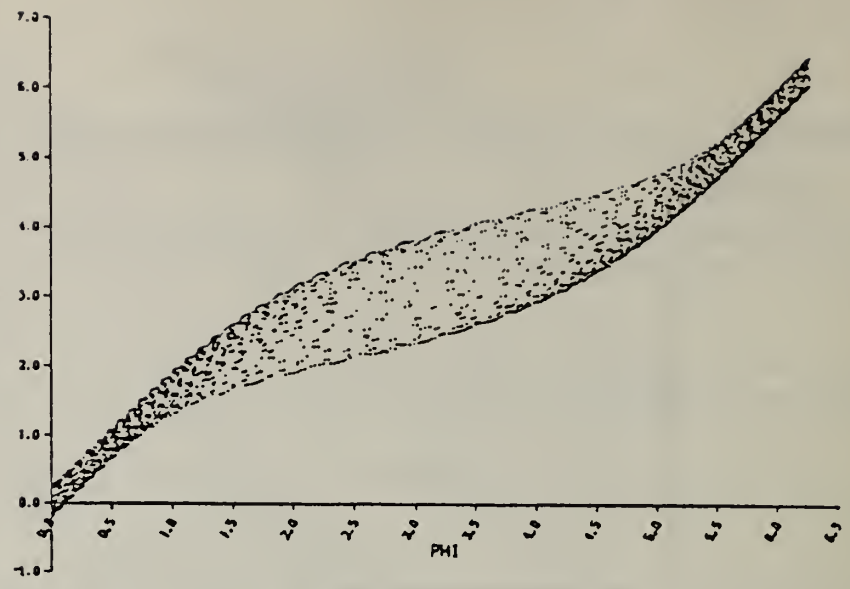

FIG. 4b

Z VS SIN OF PHI

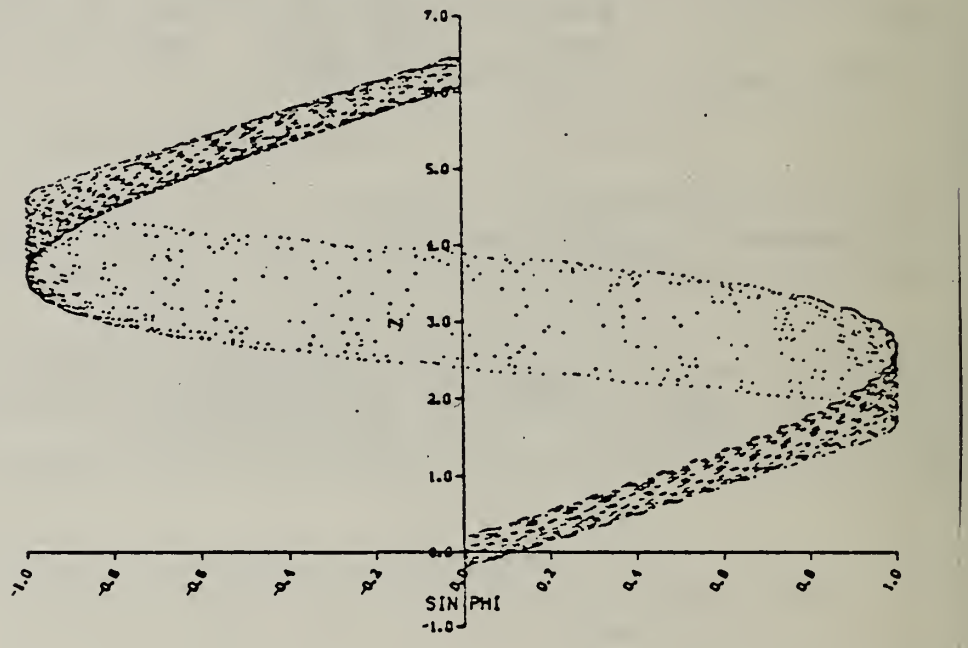

FIG. 4c

SAME AS 4b, WITH AXES EXCHANGED

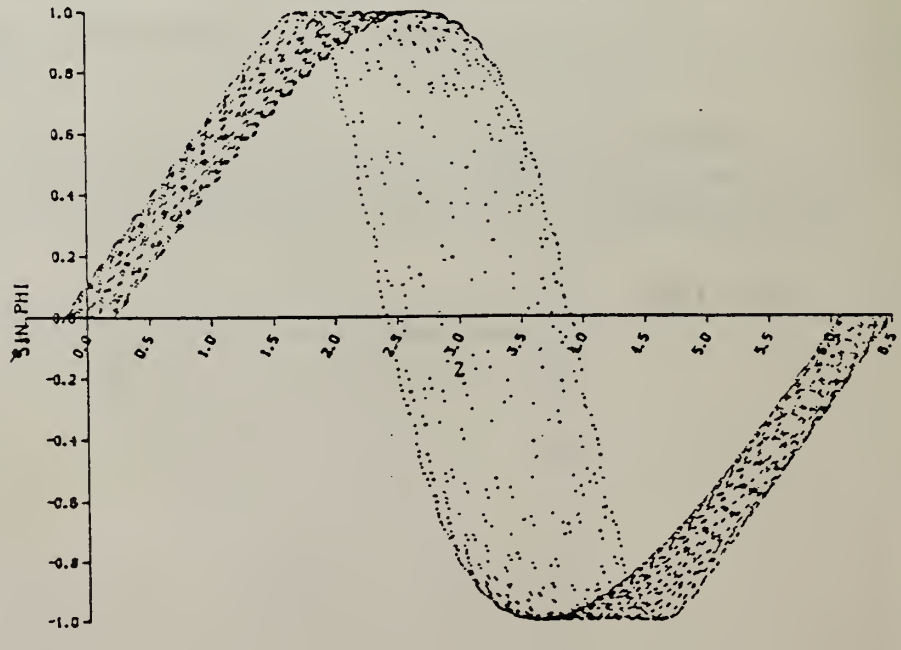

FIG. 5
COMPOSITE
POINCARÉ MAP
PHIDOT VS PHI

FOR ALL 40
START TIMES

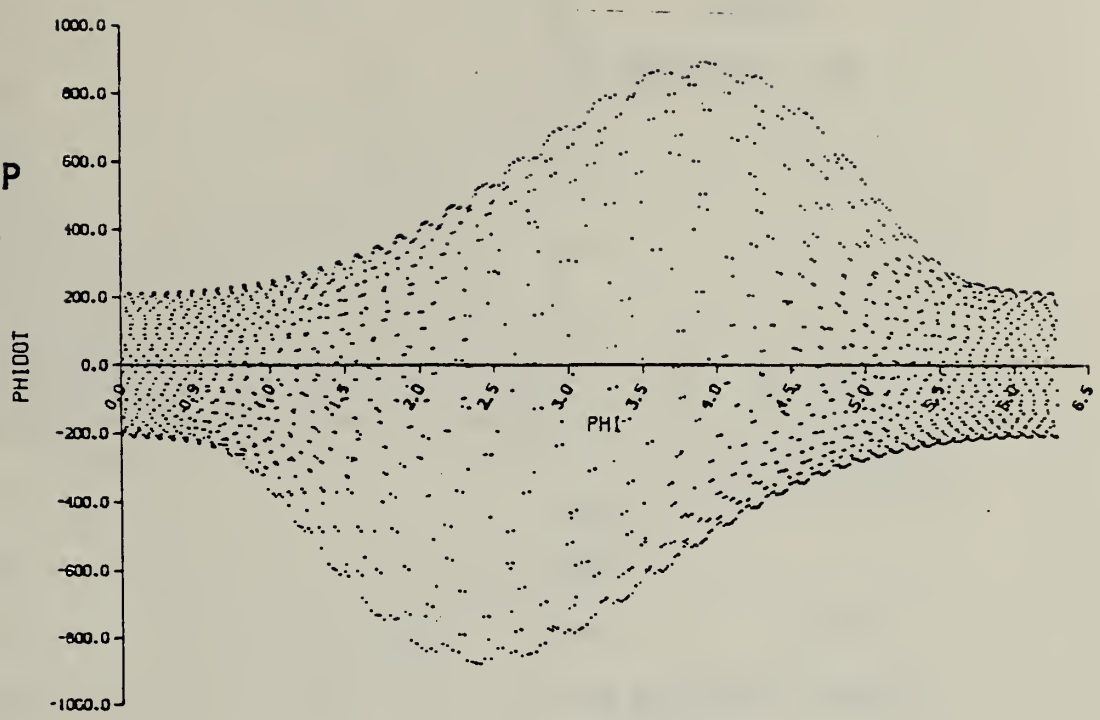

FIG. 6
PHI VS TIME

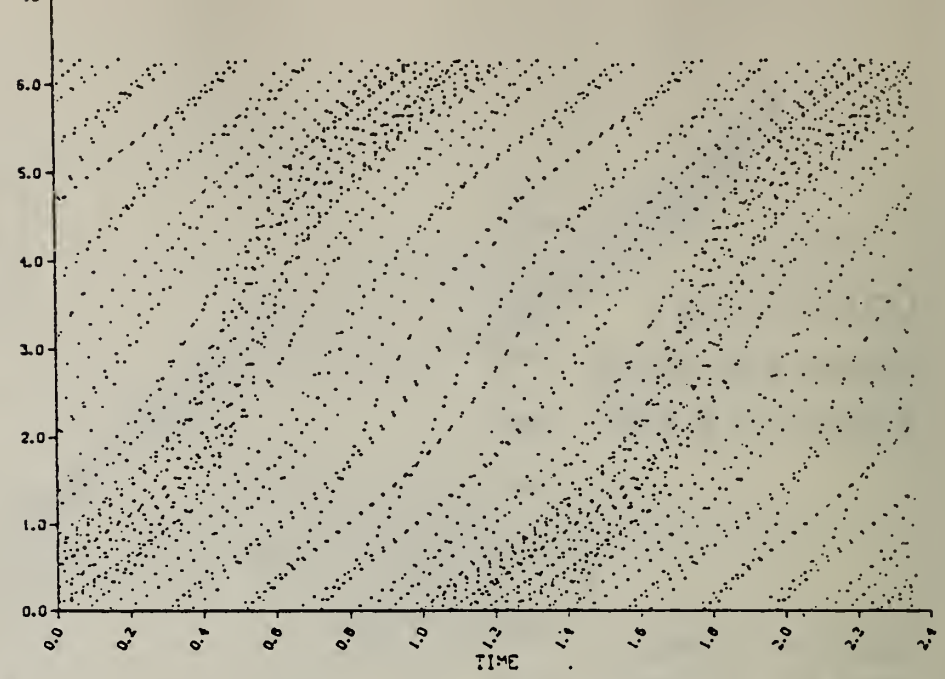

FIG. 7
PHIDOT VS TIME

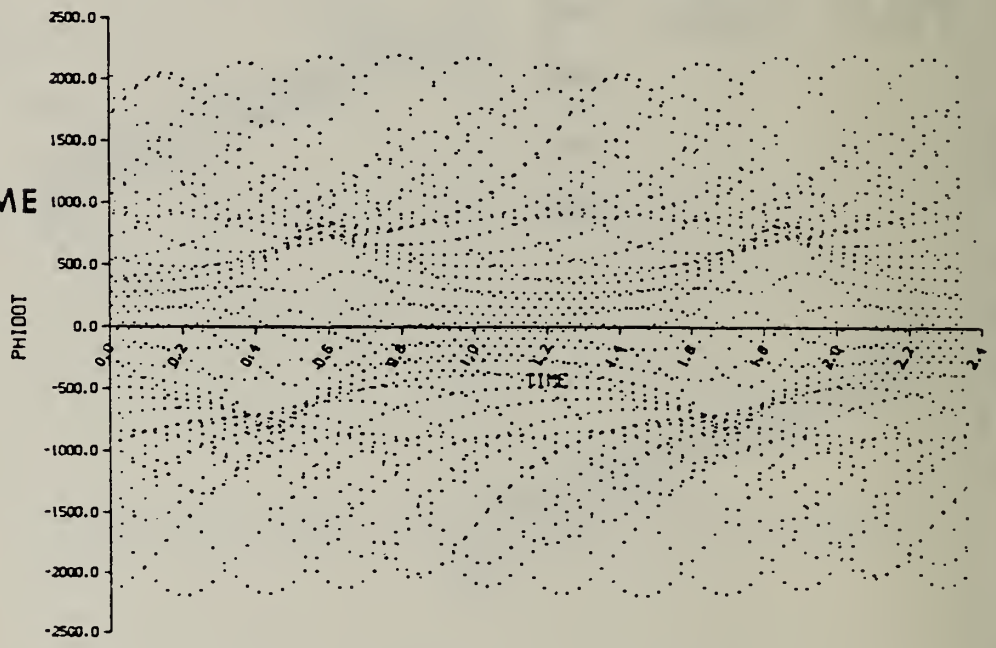

FIG. 8
SIN OF PHI
VS TIME

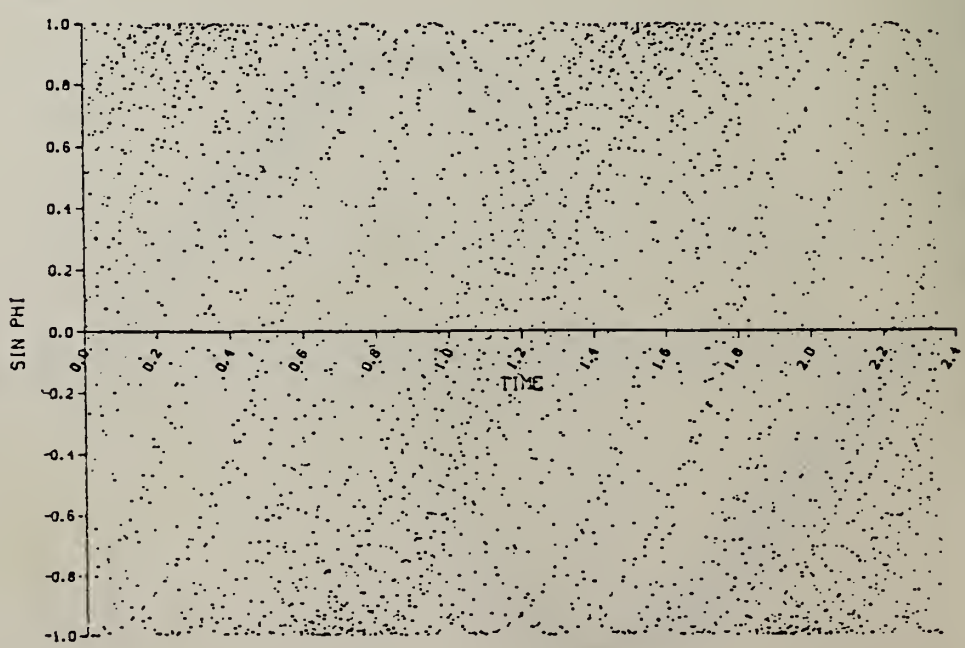

FIG. 10

COMPOSITE

POINCARÉ MAP

CF. FIG. 5

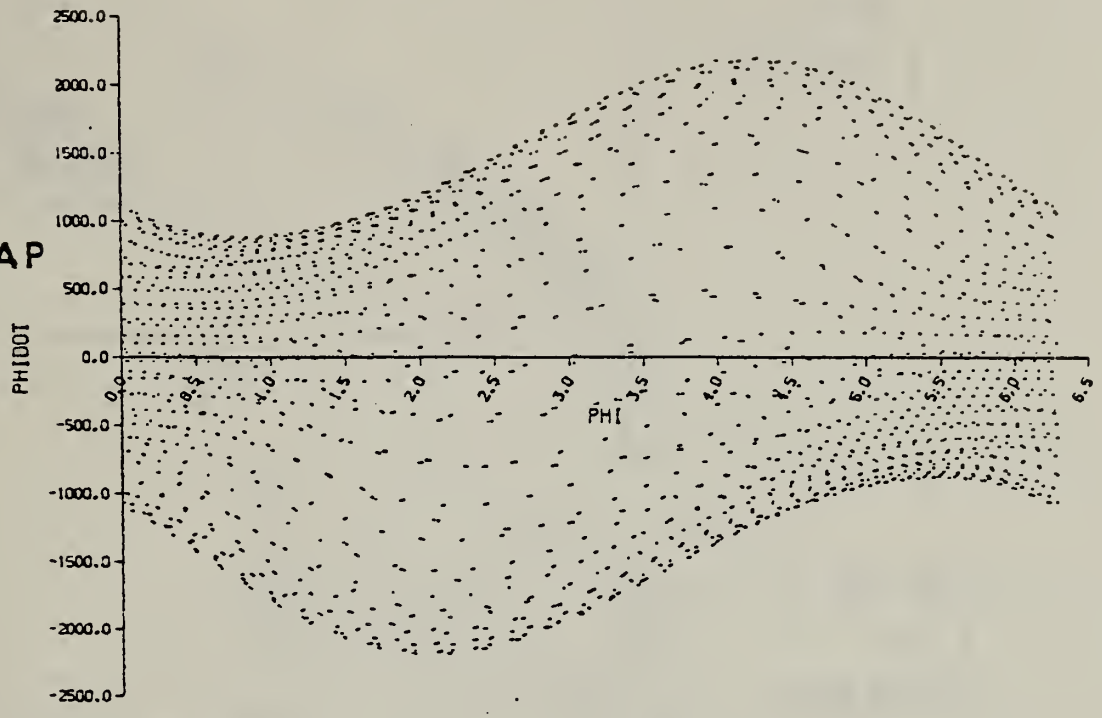

FIG. 9
Z VS PHI

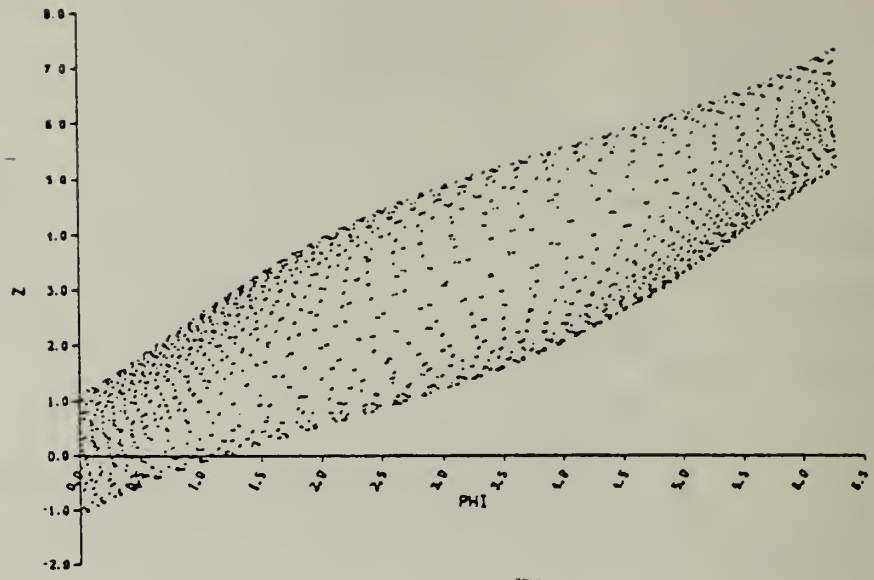

FIG. 9b
Z VS
SIN OF PHI

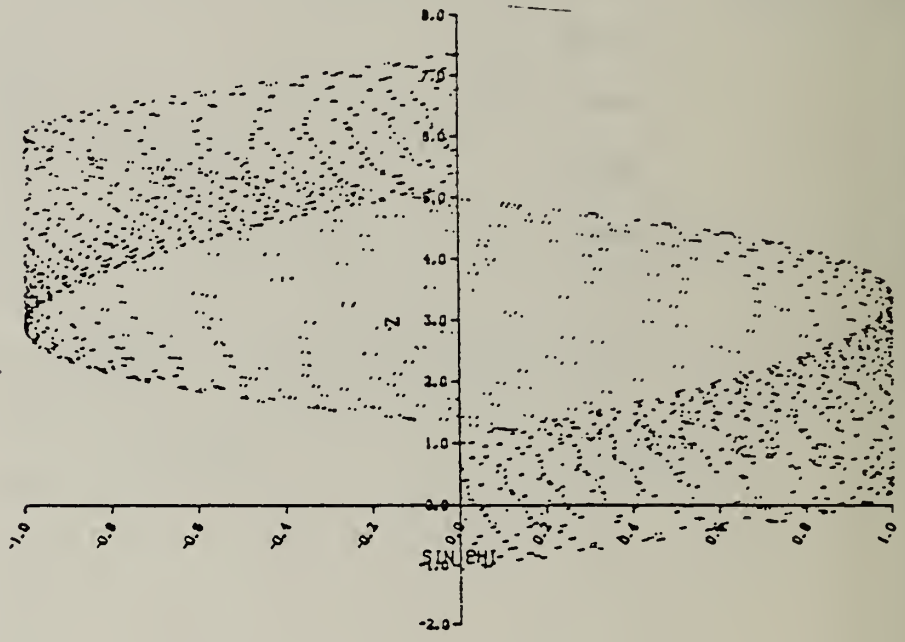

FIG. 9c
SAME AS 9b
WITH AXES
EXCHANGED

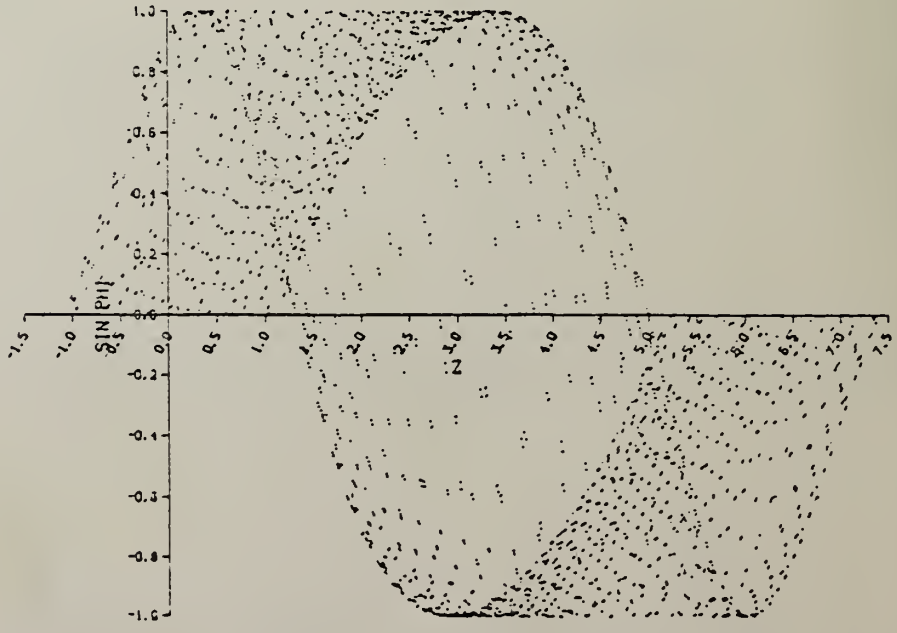

FIG. 11

PHI VS TIME
ONE POINT PER
DRIVE CYCLE

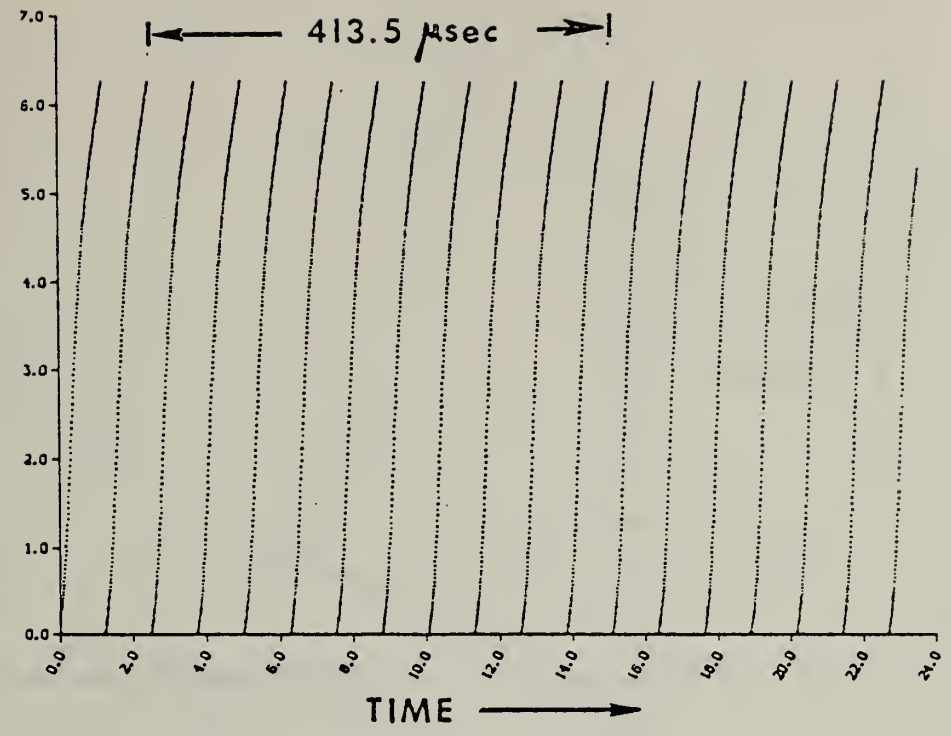

FIG. 12

PHIDOT VS TIME

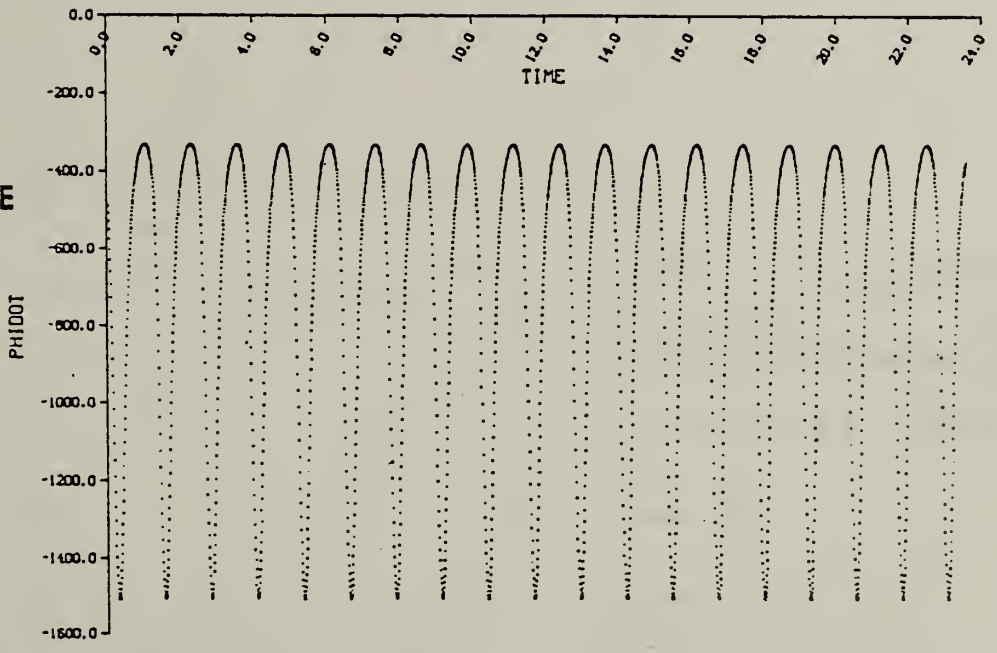

FIG. 13

SIN PHI VS TIME

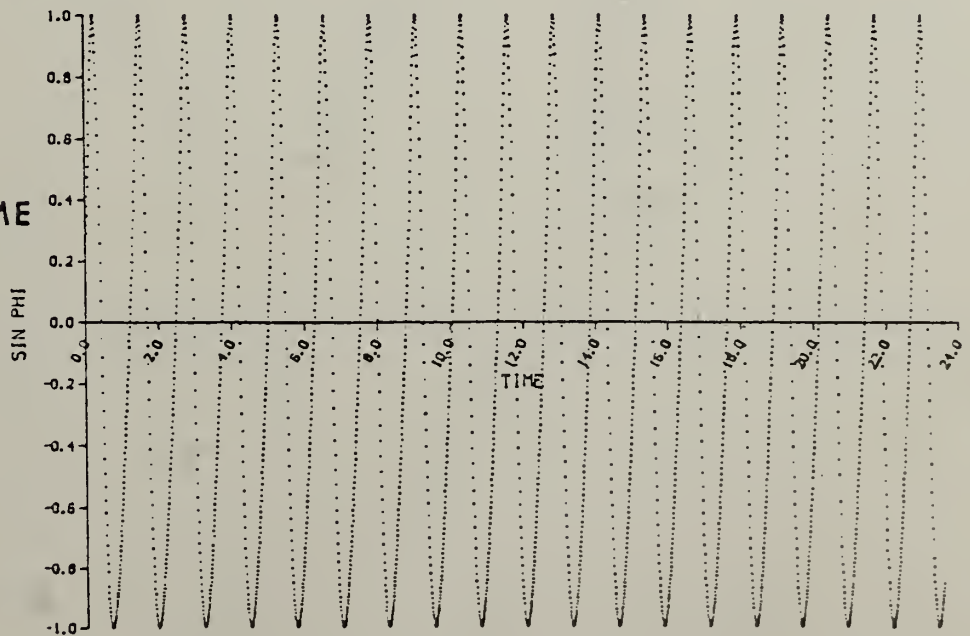

FIG. 14
Z VS PHI

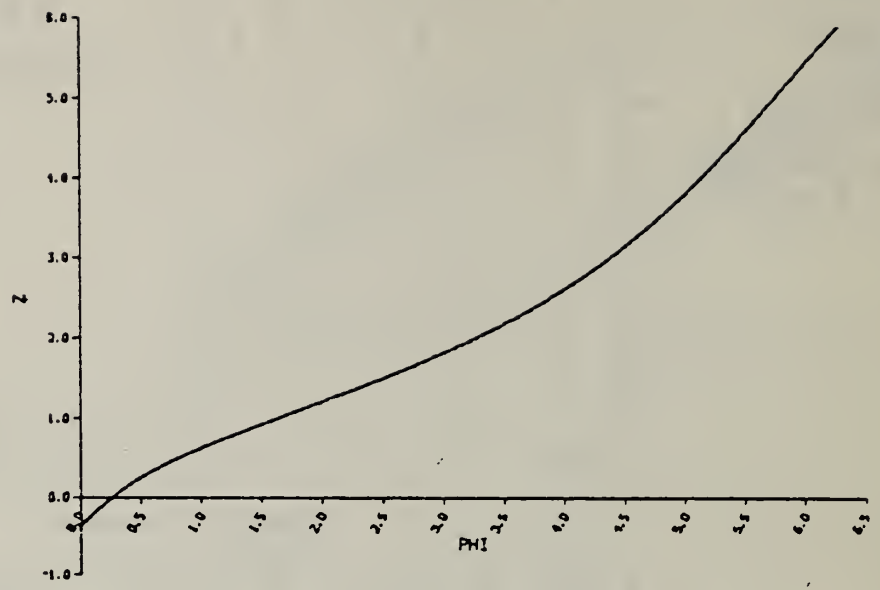

FIG. 15
POINCARÉ MAP
PHIDOT VS PHI

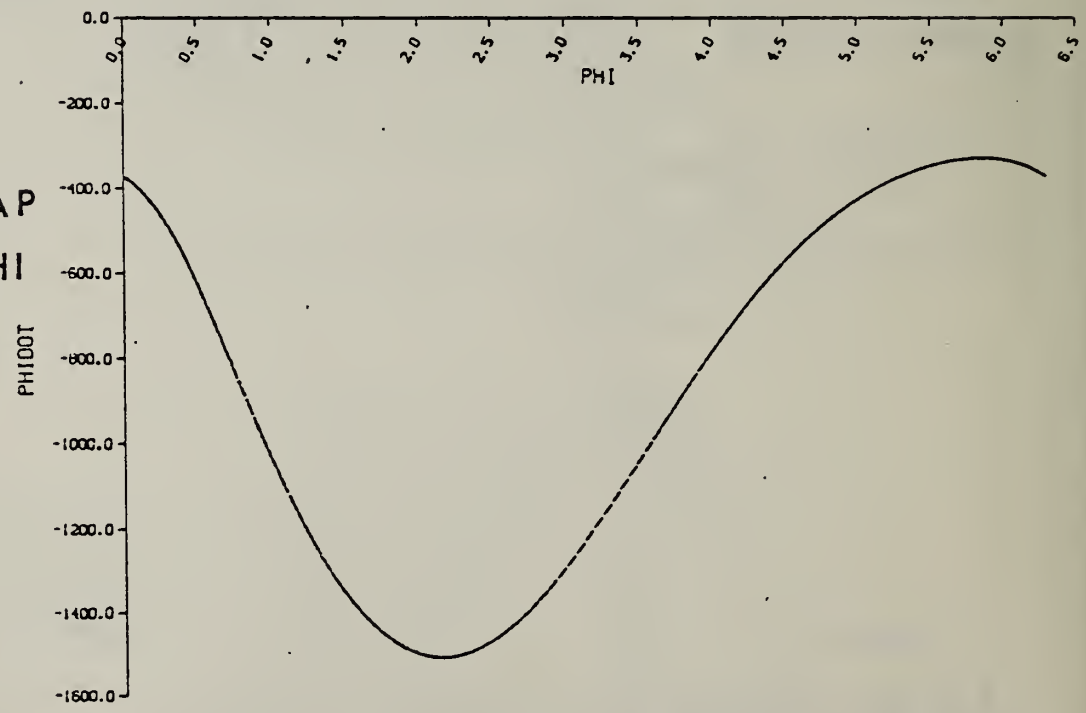

FIG. 16
PHI VS
TIME

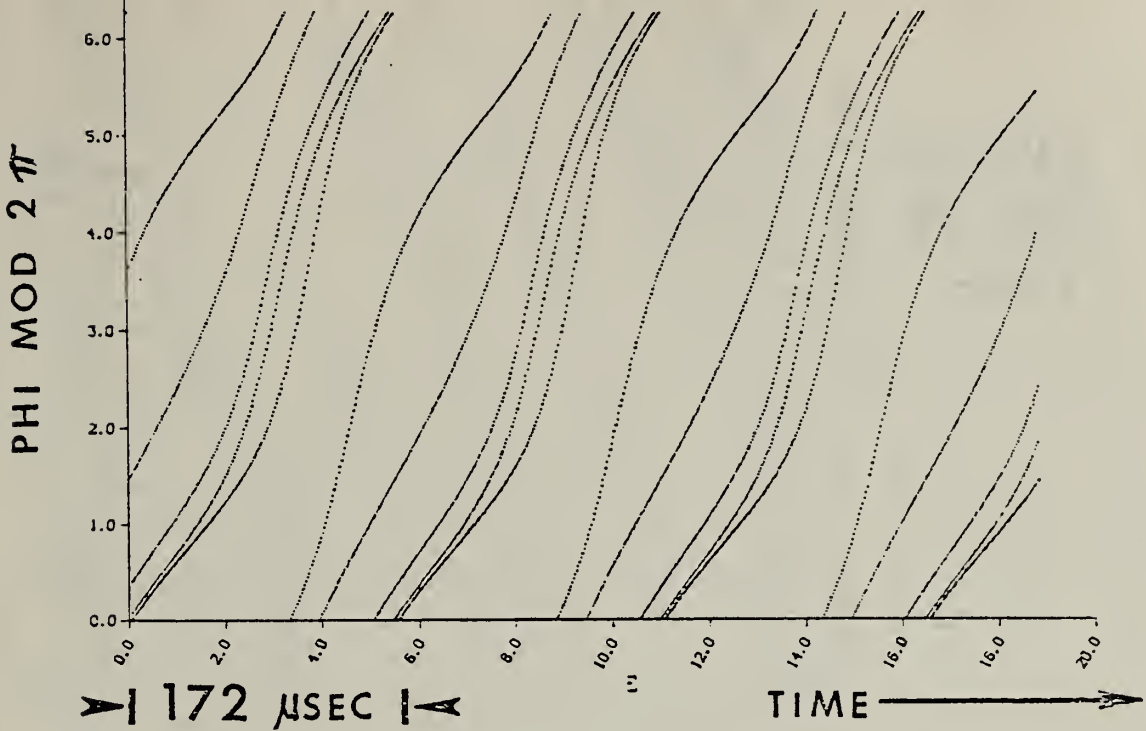

FIG. 17
PHIDOT
VS TIME

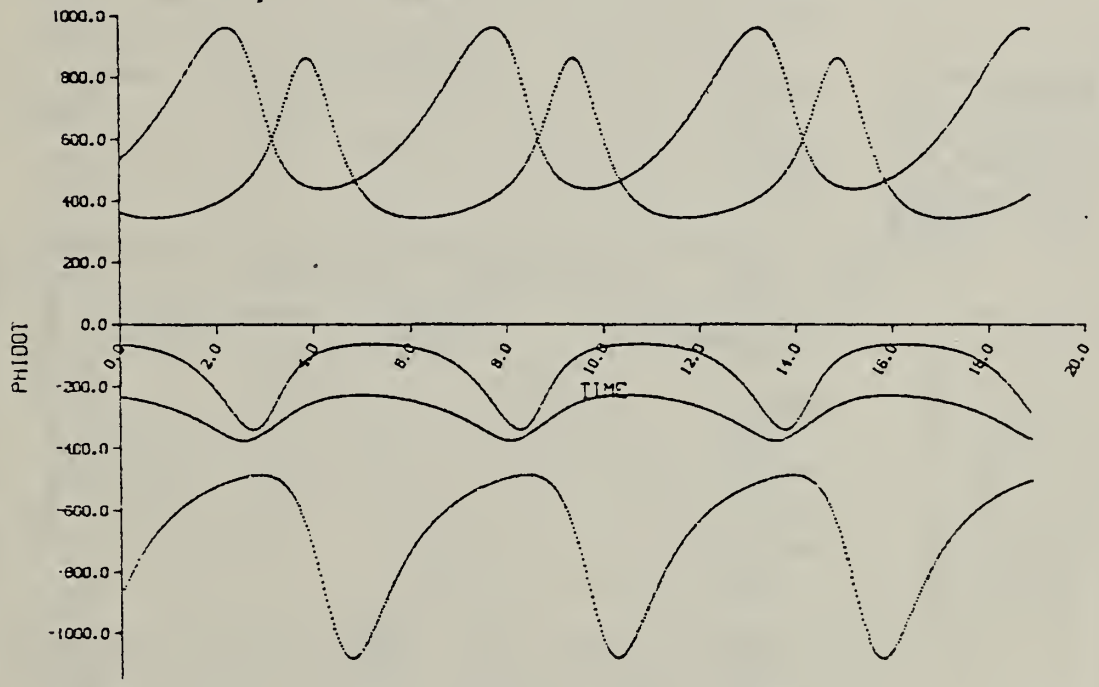

FIG 18
SIN PHI
VS TIME

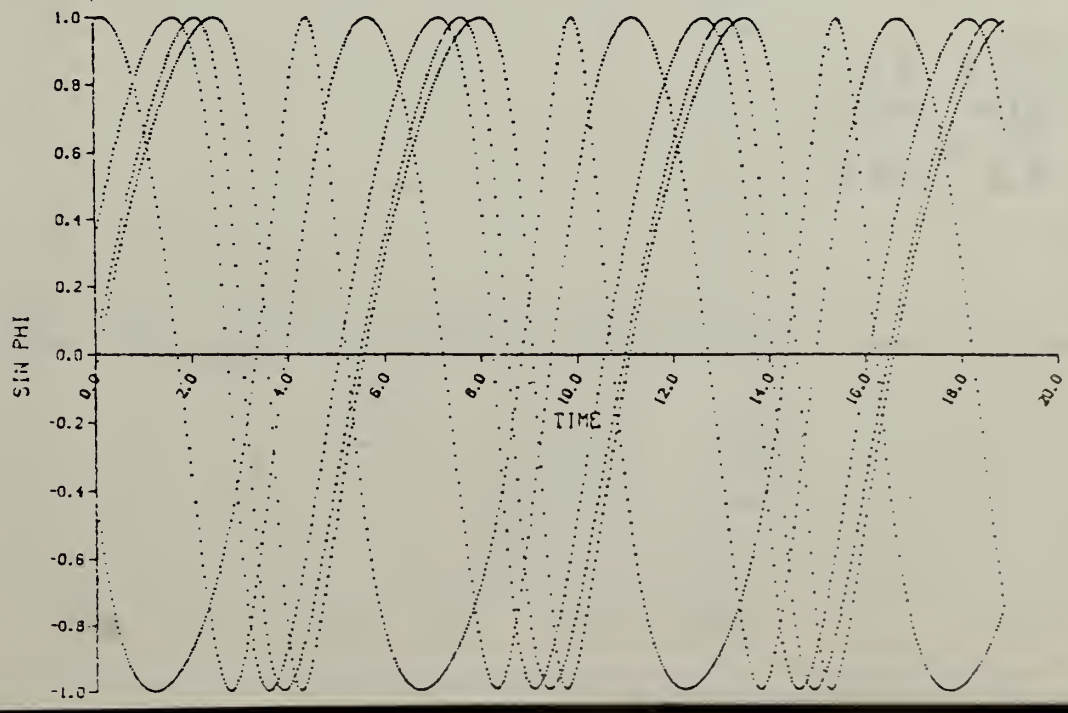

FIG. 19
PHI VS
TIME

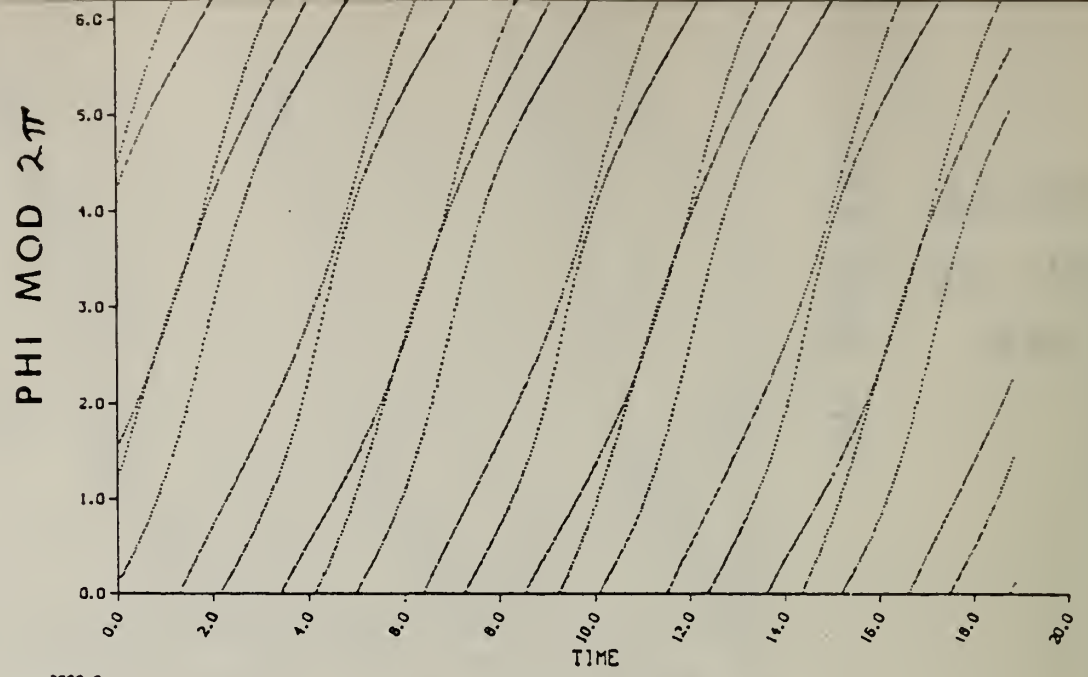

FIG. 20
PHIDOT
VS TIME

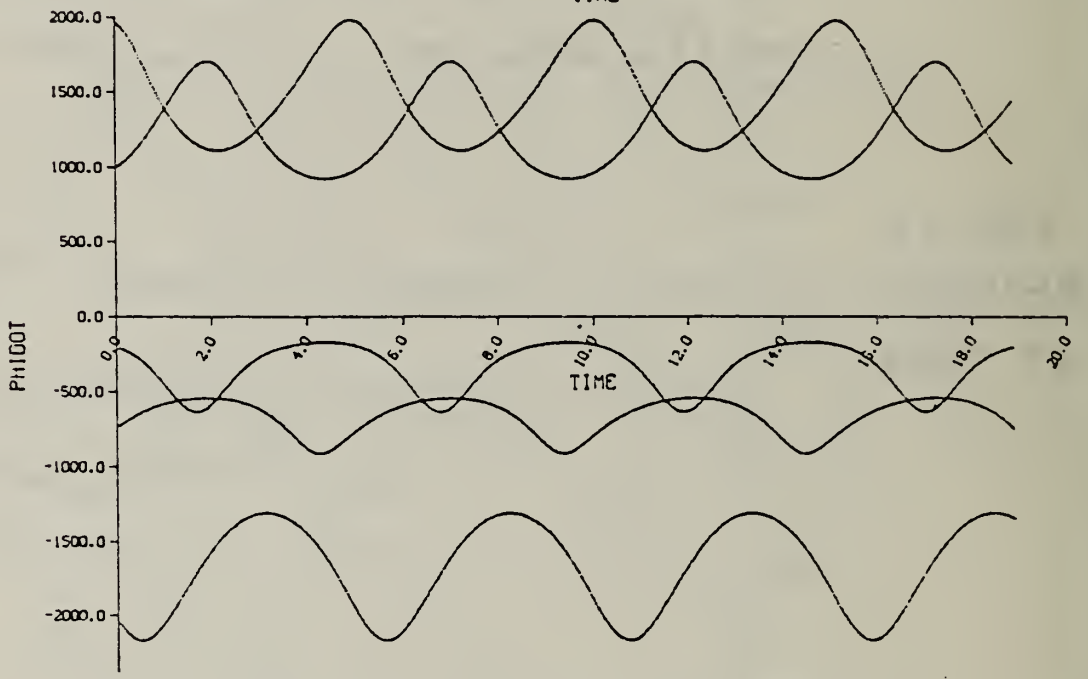

FIG. 21
SIN PHI
VS TIME

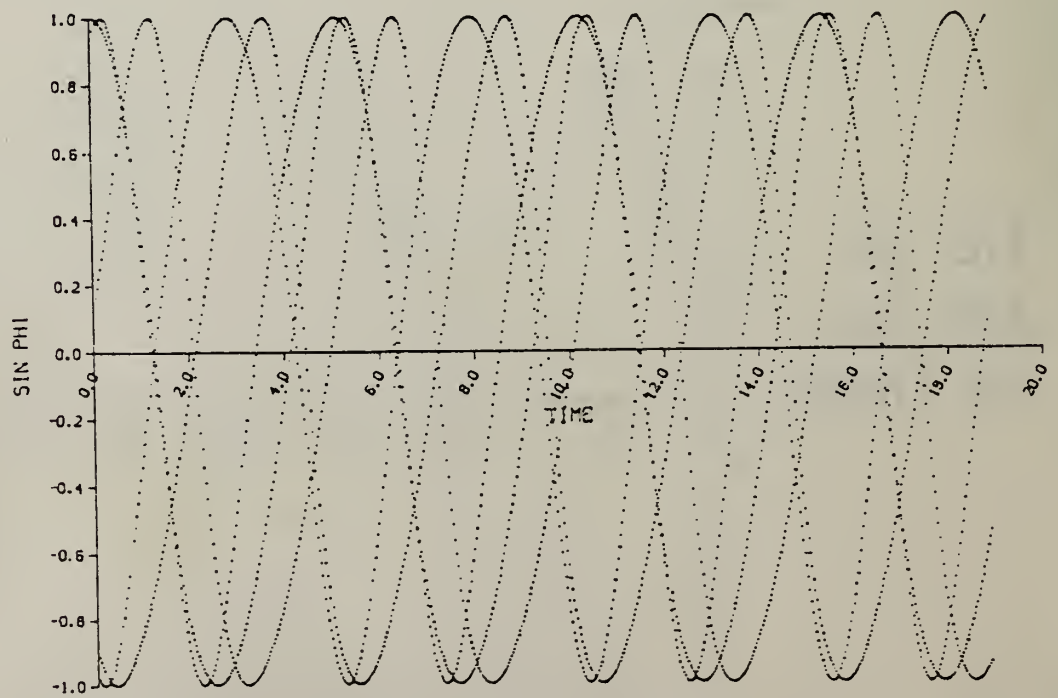

FIG. 22 RELAXATION FREQUENCY VS AMPLITUDE k OF THE DRIVE SIGNAL

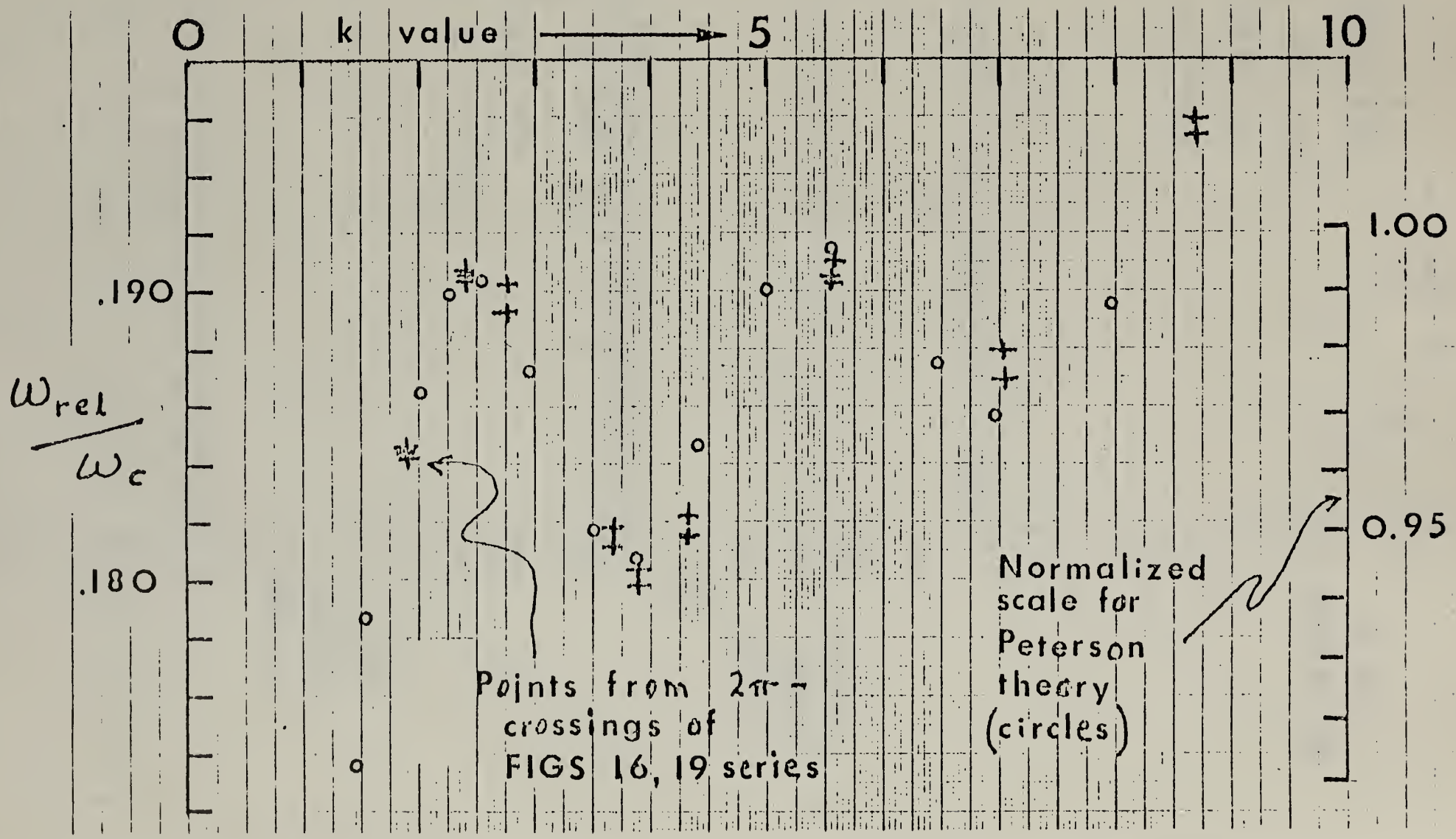

FIG. 23
PHI VS TIME

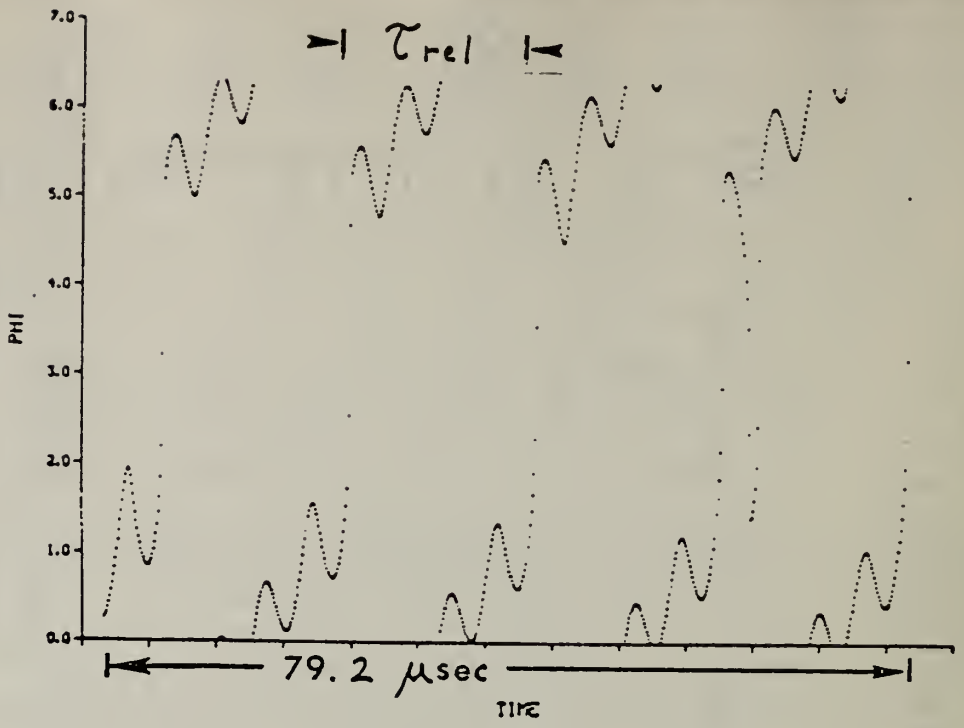

FIG. 24
PHIDOT
VS TIME

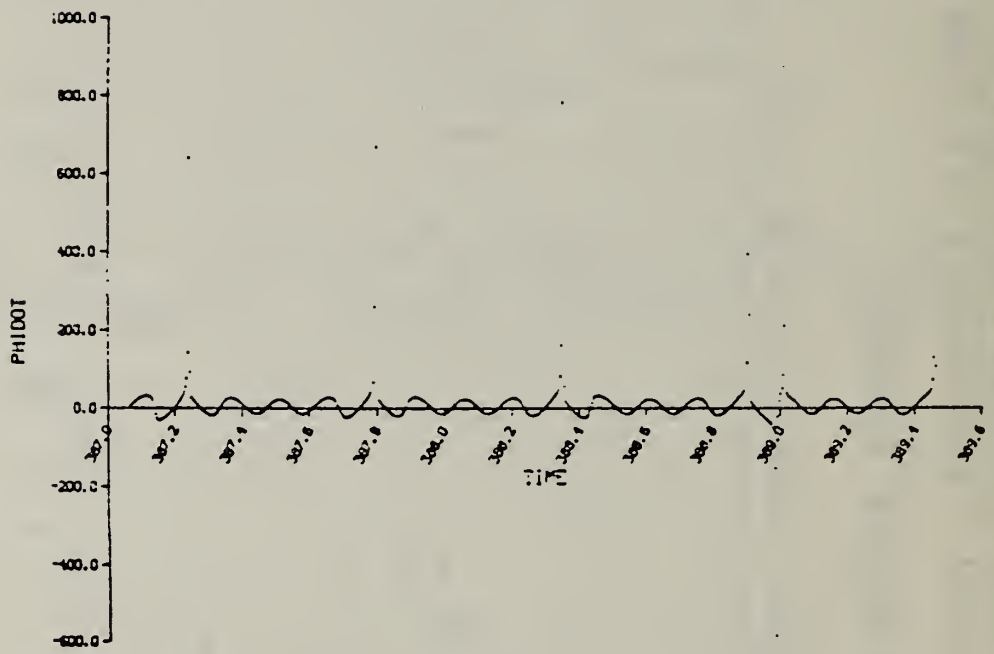

FIG. 25
SIN PHI
VS TIME

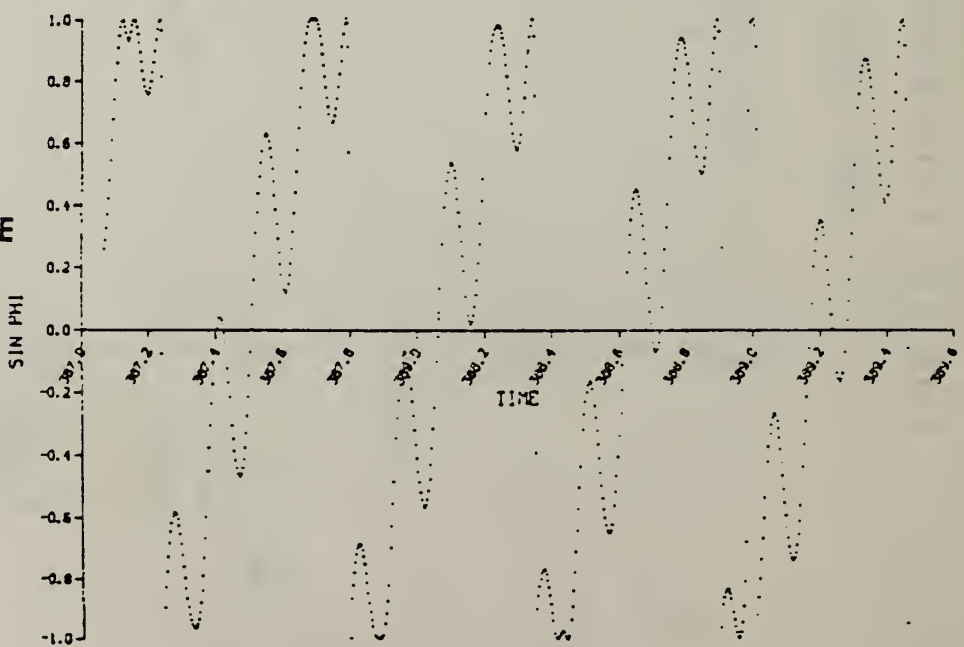

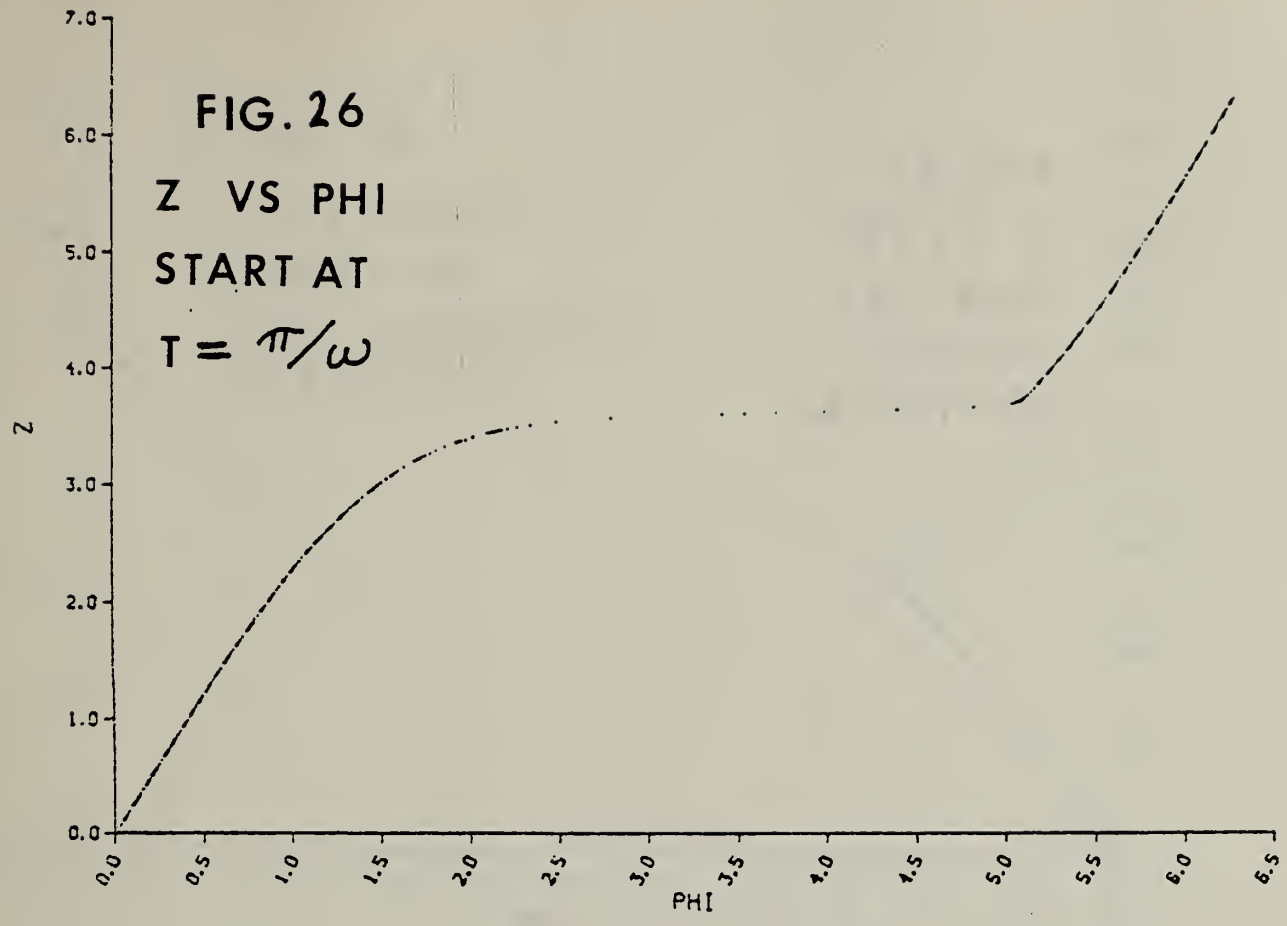
FIG. 26
Z VS PHI
START AT
T = π/ω
Z
PHI
0.0
1.0
2.0
3.0
4.0
5.0
6.0
7.0
0.5
1.5
2.5
3.5
4.5
5.5
6.5

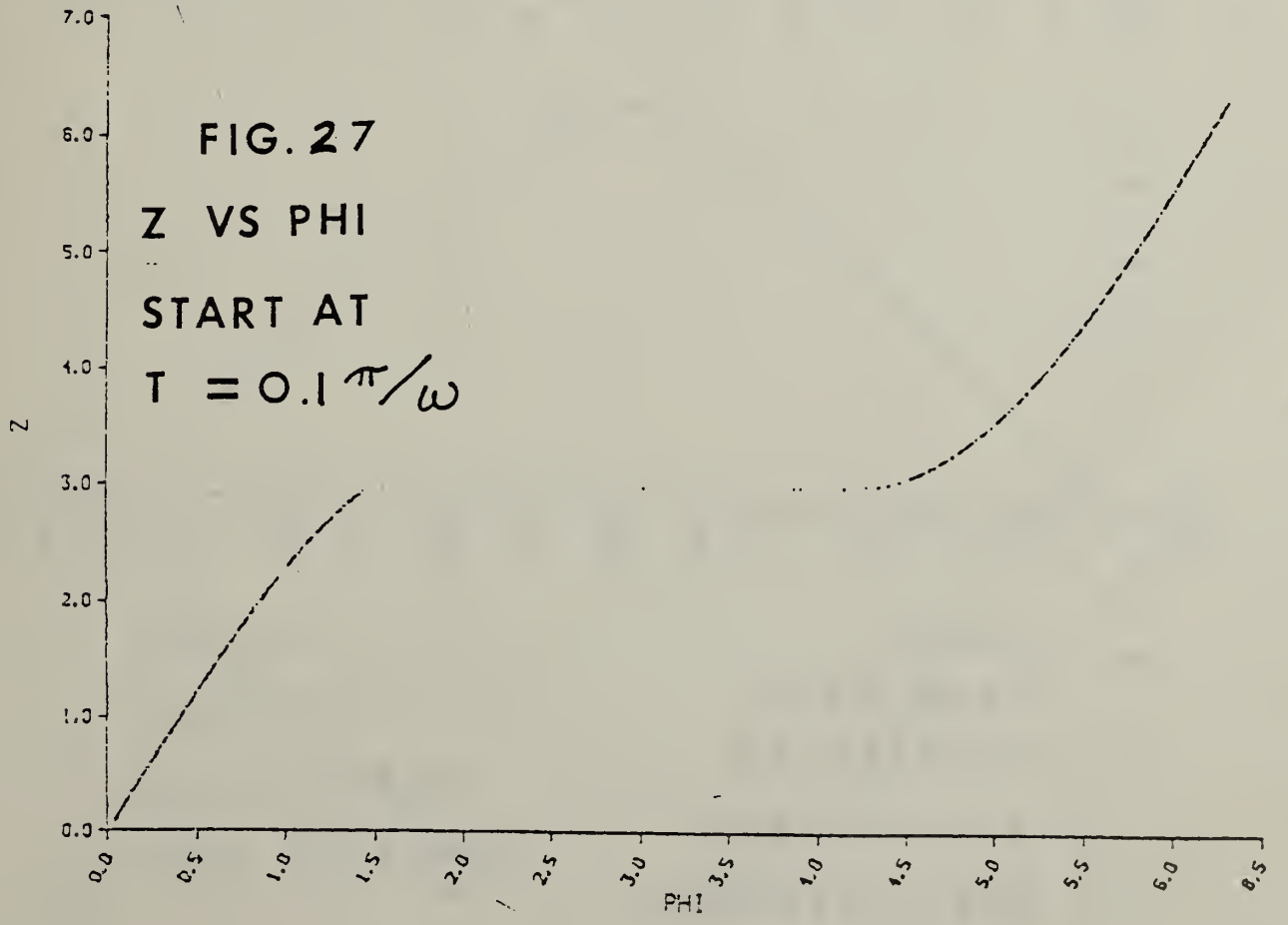
FIG. 27
Z VS PHI
START AT
T = 0.1 π/ω
Z
PHI
0.0
1.0
2.0
3.0
4.0
5.0
6.0
7.0
0.5
1.5
2.5
3.5
4.5
5.5
6.5

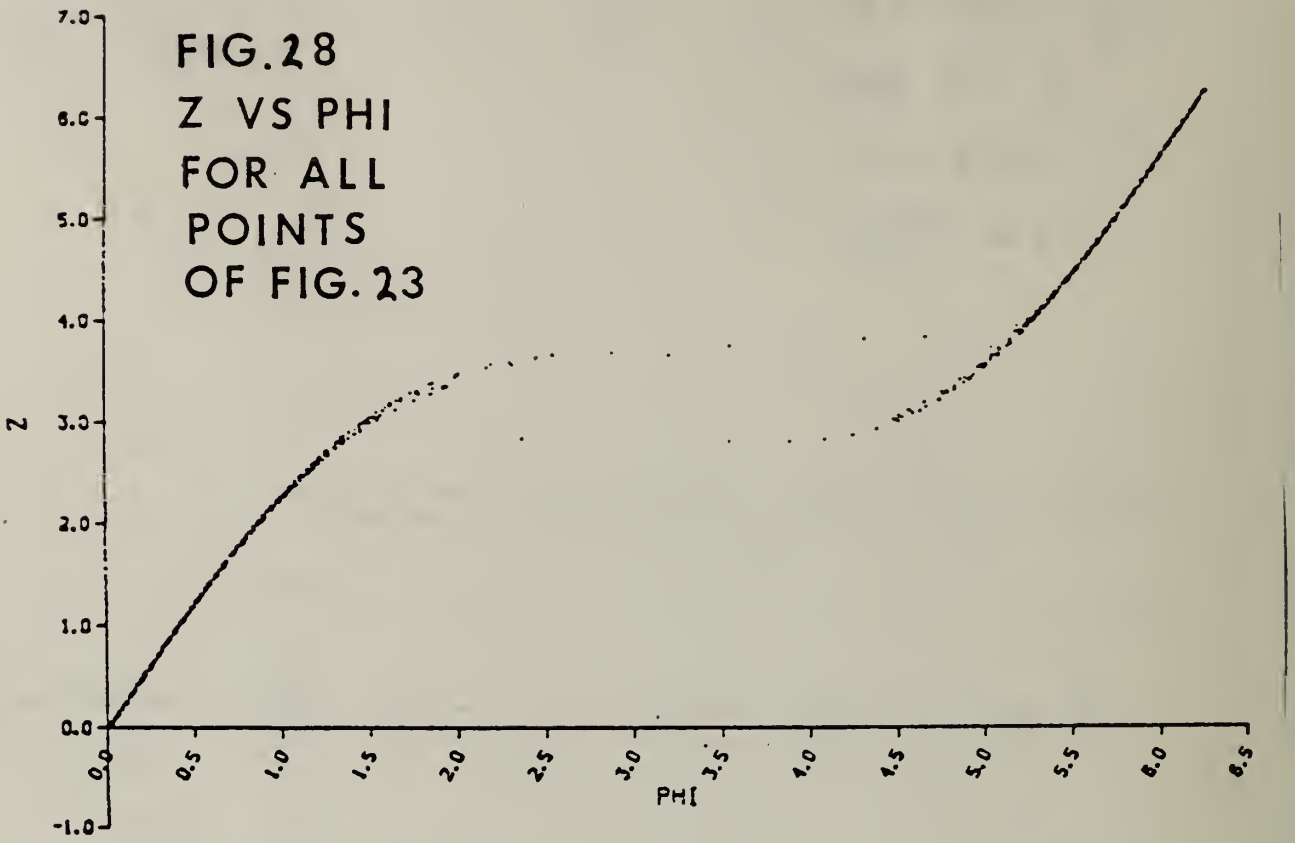

FIG. 28
Z VS PHI
FOR ALL
POINTS
OF FIG. 23

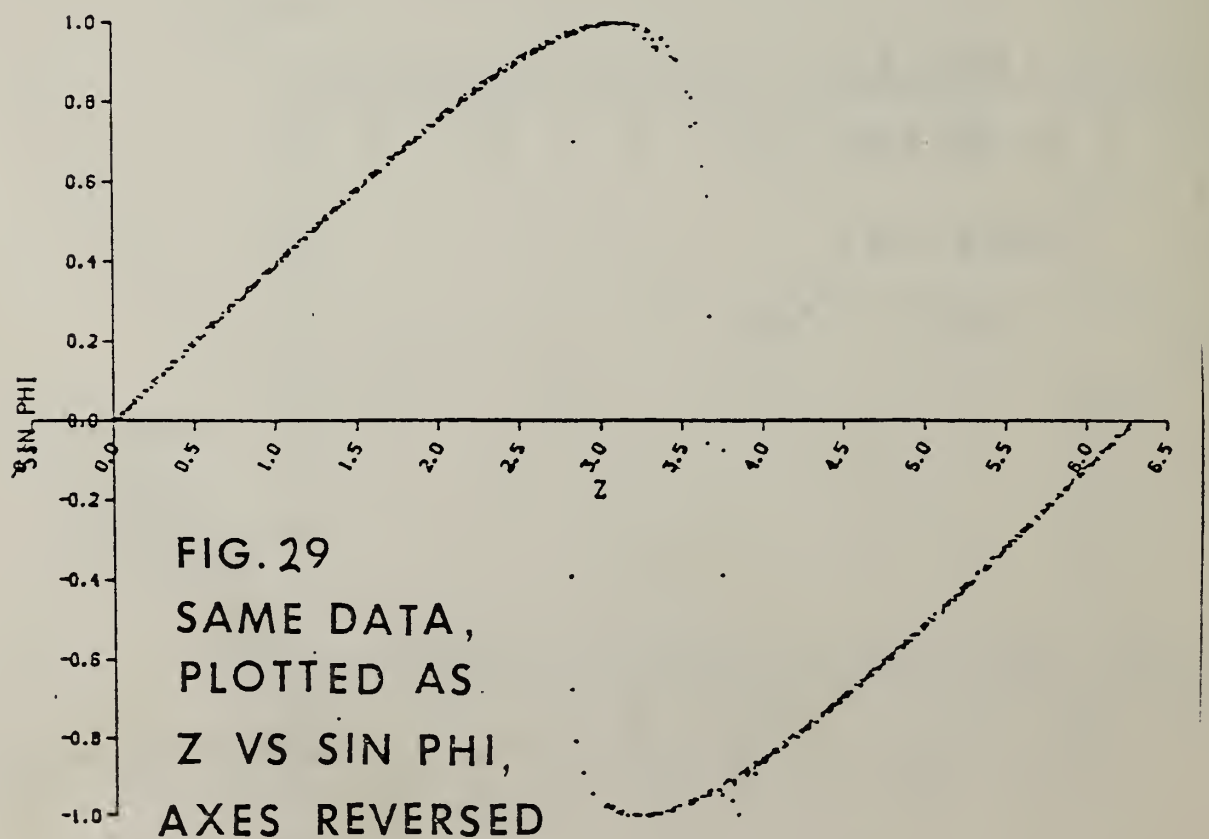

FIG. 29
SAME DATA,
PLOTTED AS
Z VS SIN PHI,
AXES REVERSED

FIG. 30

Z VS PHI AT START OF RUN, SHOWING TRANSIENTS

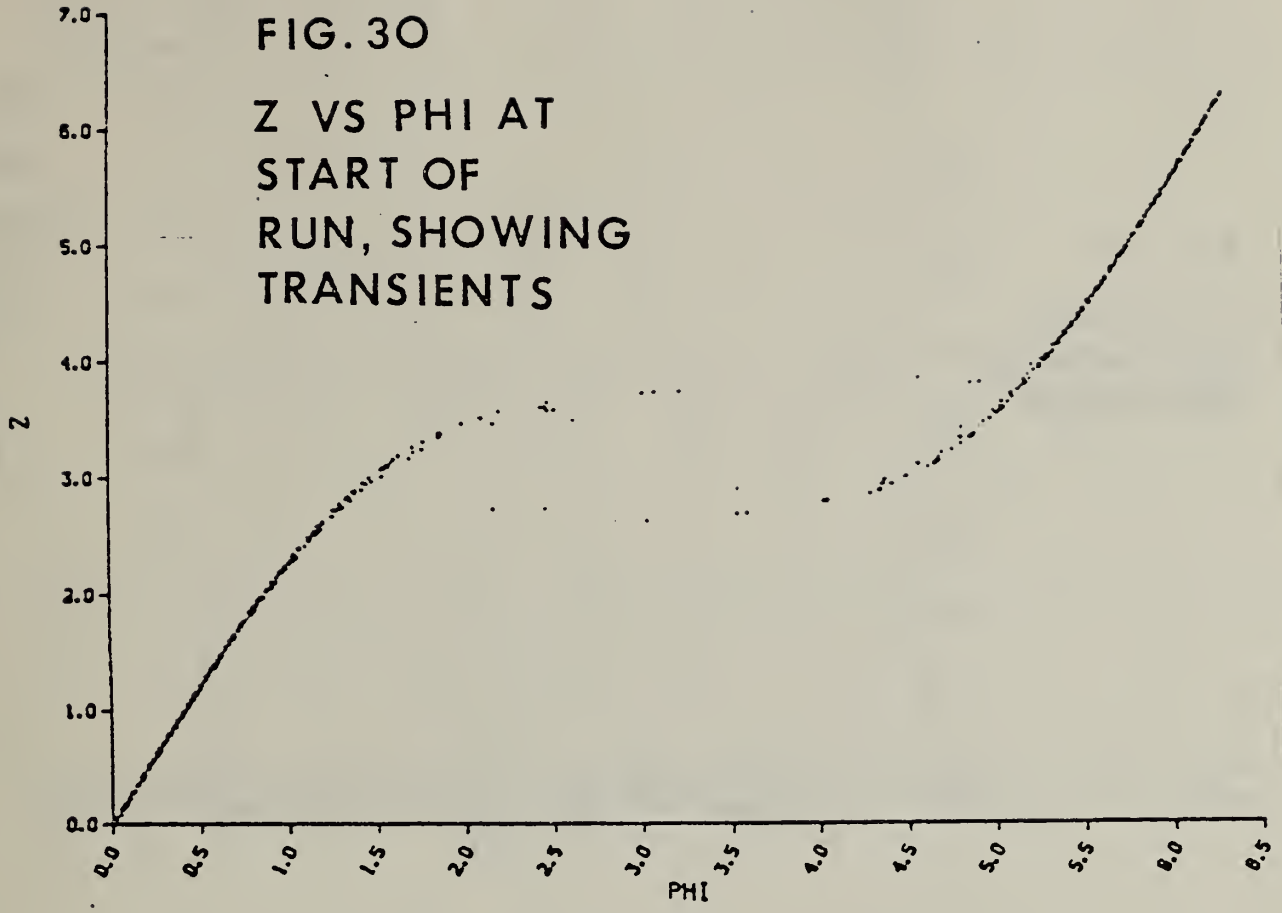

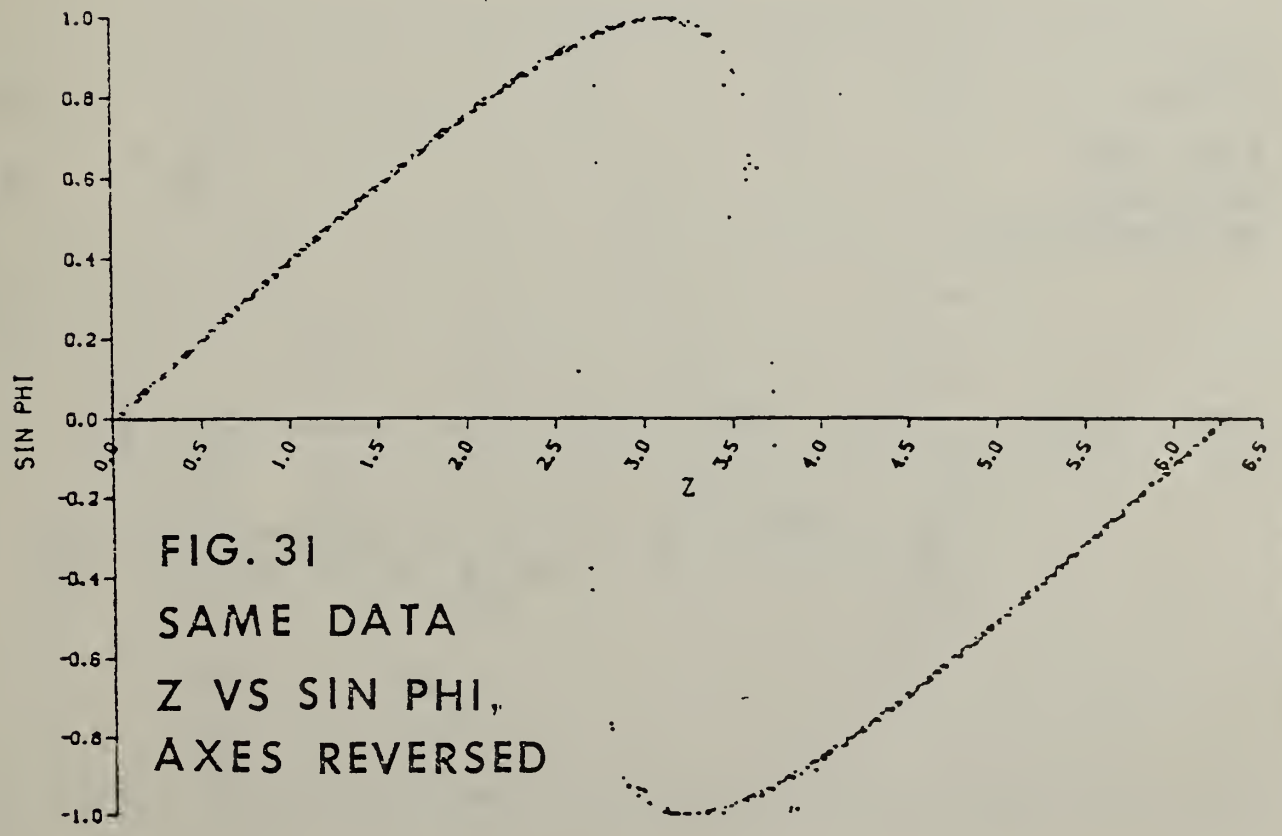

FIG. 31

SAME DATA

Z VS SIN PHI, AXES REVERSED

FIG. 32

Z VS TIME
FOR DATA OF
FIGS. 30-31

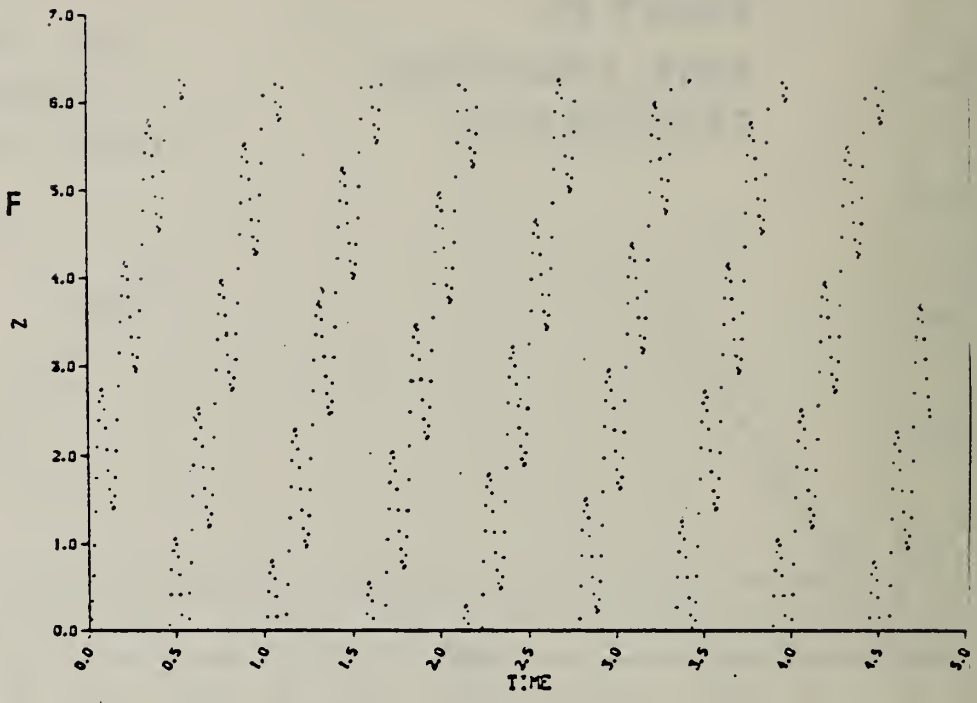

FIG. 33

Z VS TIME
FOR DATA
OF FIGS. 23-25

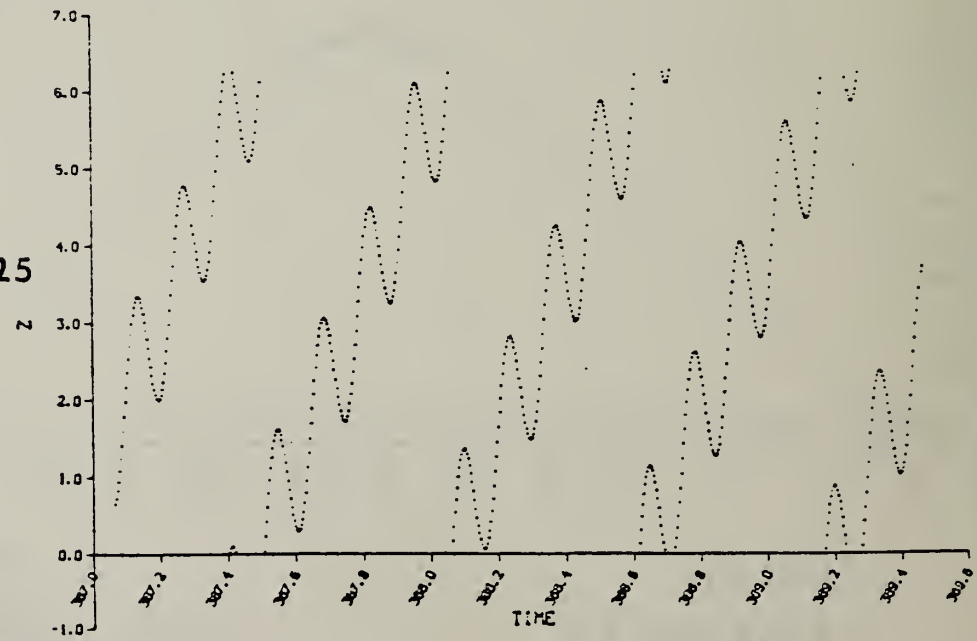

FIG. 34
SIN PHI
VS TIME:
$\gamma = 1.5$,
LONG
TIME
SCALE

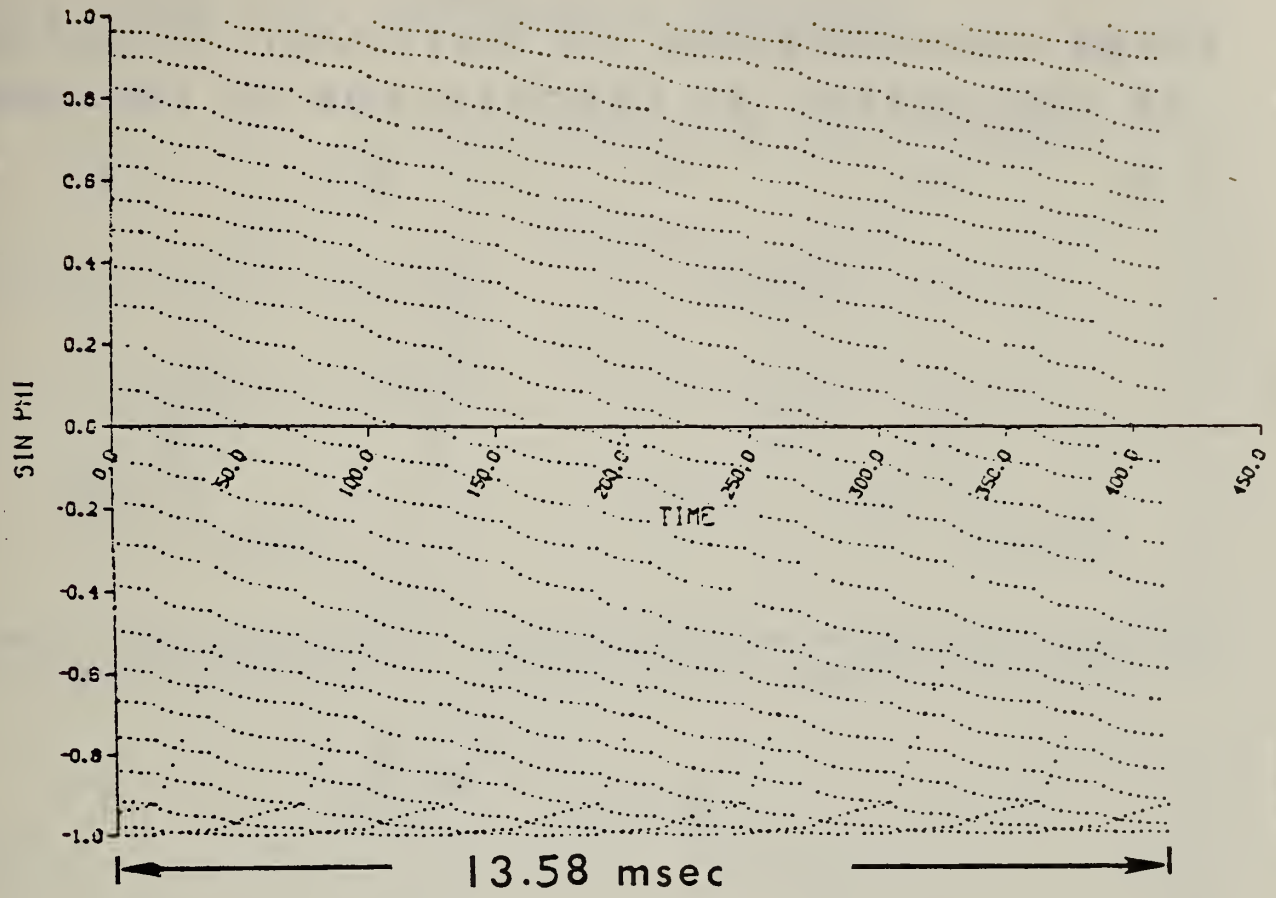

FIG. 35
SAME,
FOR
$\gamma = 0.5$

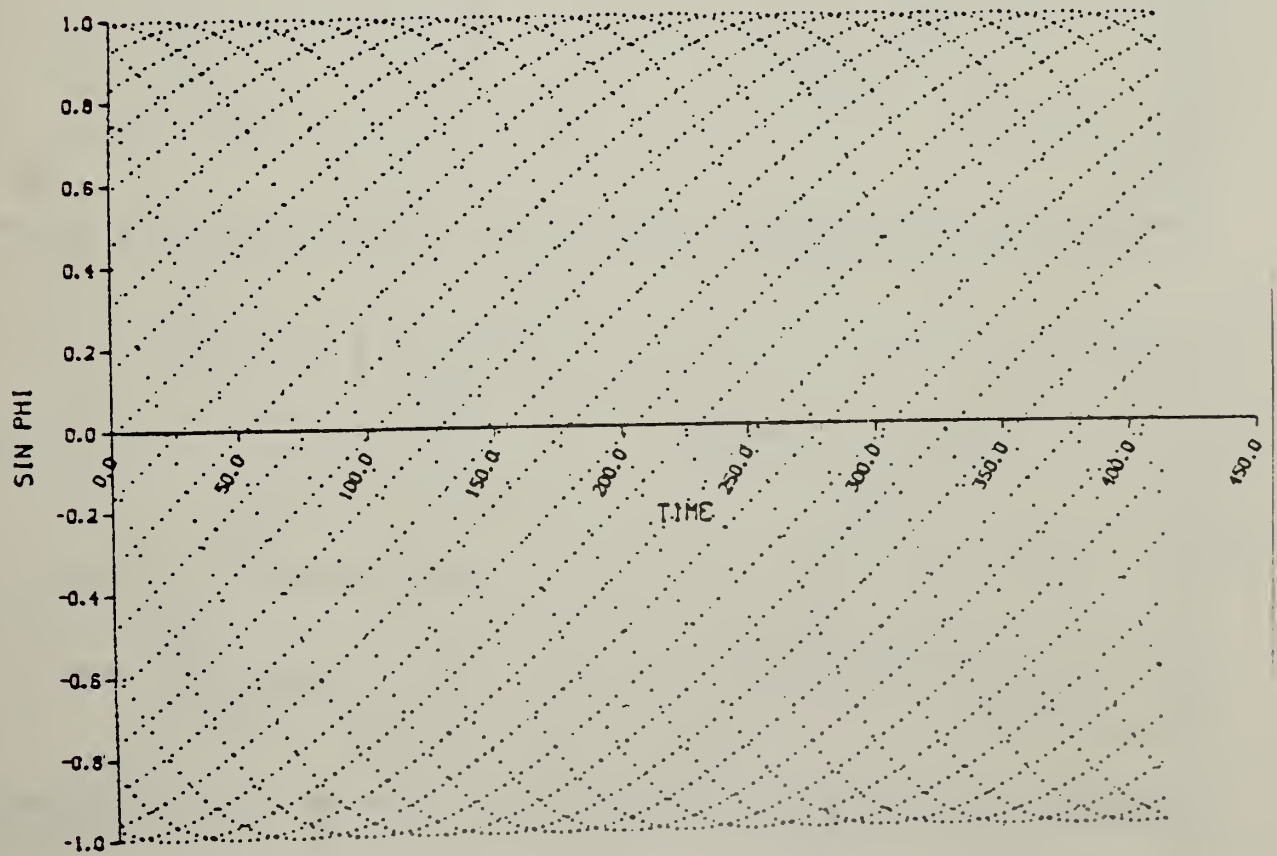

FIG.36 CONFIRMATION OF WAVEFORM VARIATION AS CALCULATED BY SANDERS FOR $\omega = 45.68128$

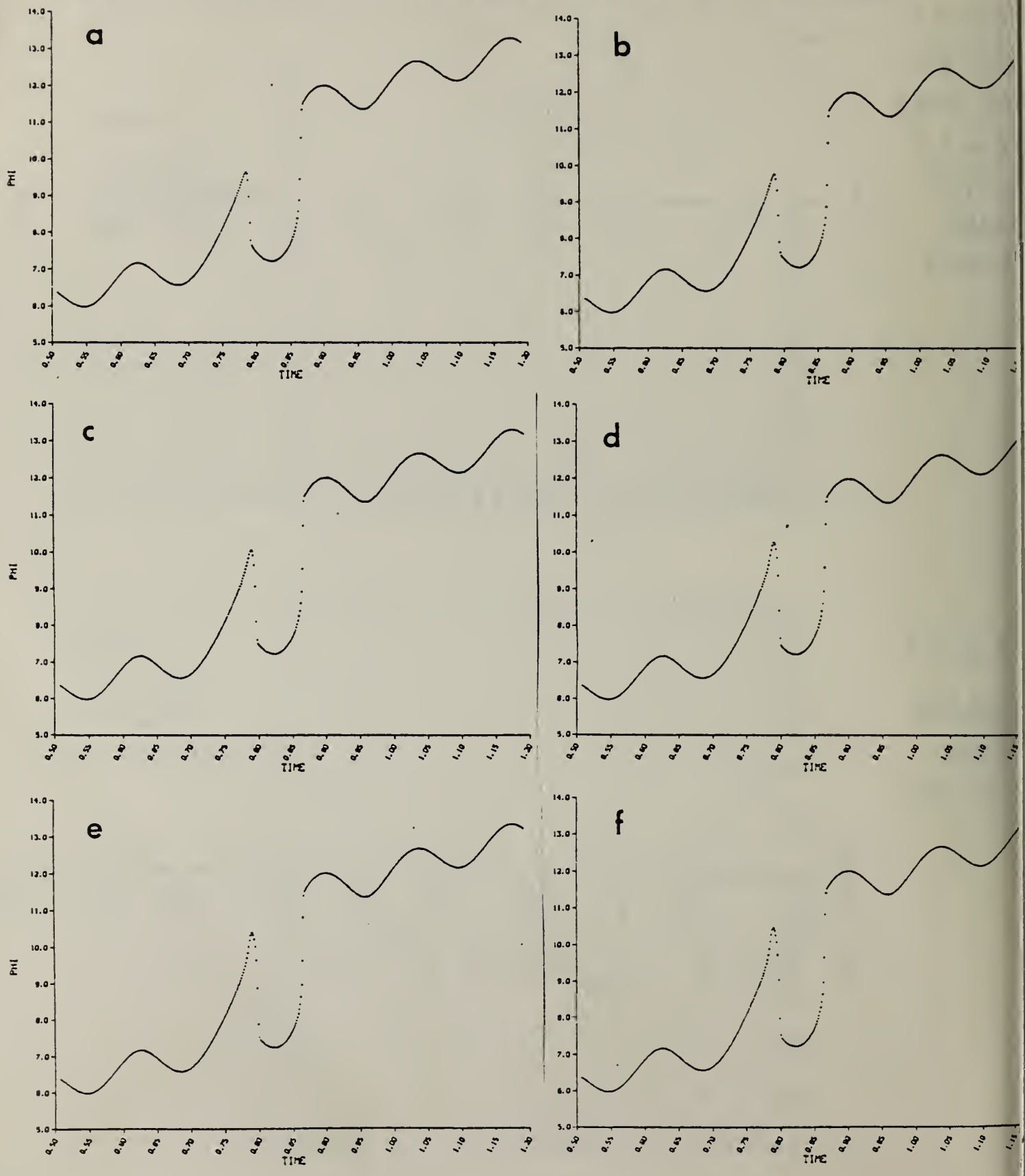

FIG. 37 SANDERS'S RESULTS

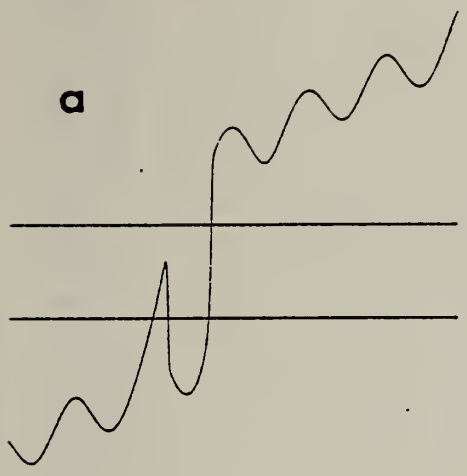

Y(TO) = 6.374423 DY(TO)= 10.0000

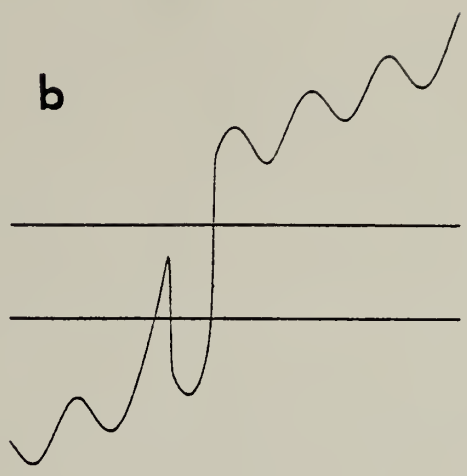

Y(TO) = 6.374424 DY(TO)= 10.0000

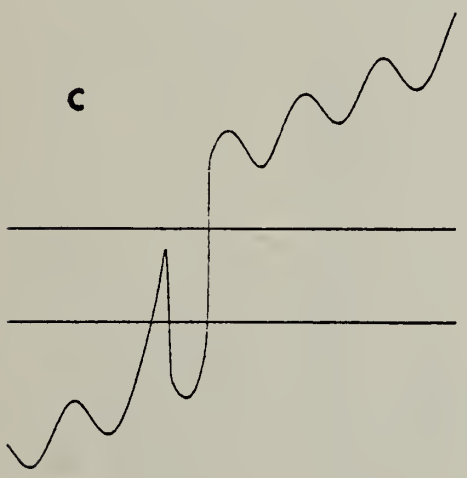

Y(TO) = 6.374425 DY(TO)= 10.0000

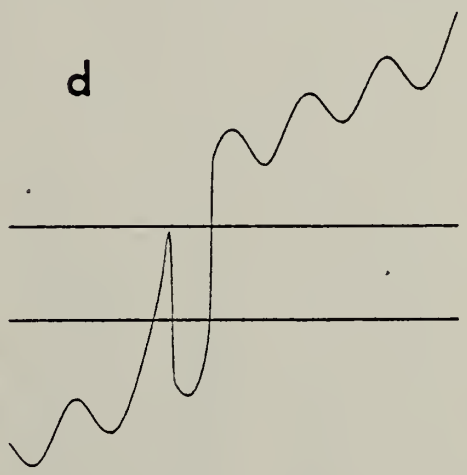

Y(TO) = 6.374426 DY(TO)= 10.0000

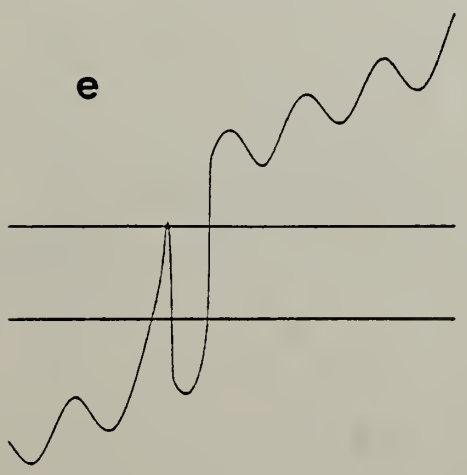

Y(TO) = 6.374427 DY(TO)= 10.0000

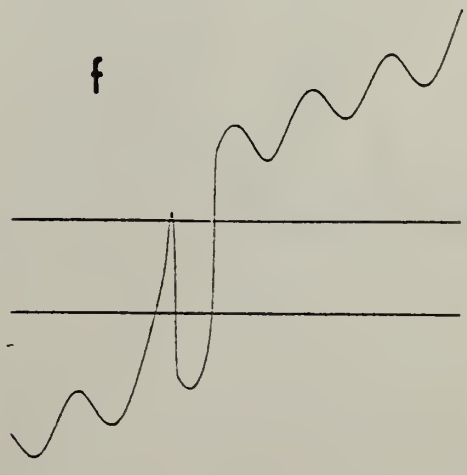

Y(TO) = 6.374428 DY(TO)= 10.0000

Appendix A.

User Guide to the program CUSHEQ

```
10      Usage of CUSHEQ/DOUBLE in CTS
20
30      I.  Execution
40          A.  On-line execution
50              1.  Enter CTS
60                  >@CTS
70              2.  Assign a temporary file.
80                  ->PXQT ASG.T 7
90              3.  Execute the program
100                  ->XQT CUSHEQ/DOUBLE
110                You will need the following information:
120                   1.  The unit number for writing the output
130                       (the same number you assigned in A.2.)
140                   2.  A, B, C, D, E, and W
150                   3.  S (Integration step, STEP = S * TWOPI / W)
160                   4.  Number of times to repeat integration
170                   5.  0 for MOD PHI by 0
180                       1 for MOD PHI by 2PI
190                   6.  Whether or not PHI should be divided by T.
200                   7.  Whether or not the arrays should be saved for graphing.
210                       (If the answer is no, only the last point is saved.)
220                   8.  Coordinates of the starting pt,
230                   9.  Accuracy desired
240                  10.  Start time to send to the integrator
250
260          B.  To execute by batch.
270              1.  Use the data file JOSEPH*DATA.
280              2.  Create an element, JOSEPH*DATA.someelementname2, with
290                  the following:
300                  line
310                    1.  7
320                    2.  A, B, C, D, E, and W
330                    3.  S (Integration step, STEP = S * TWOPI / W)
340                    4.  Number of times to repeat integration
350                    5.  0 for MOD PHI by 0
360                        1 for MOD PHI by 2PI
370                    6.  Coordinates of the starting pt.
380                    7.  Accuracy desired
390                    8.  Start time to send to the integrator
400
410              Sample element:
420                     10 7
430                     30 11. 1.e-3 1.5 1. 45.68 45.68
440                     40 1.
450                     50 0
460                     60 3000
470                     70 0. 0.
480                     80 1.e-8
490                     90 0.
500                     100 1
510              4.  Create a runstream and store it in an element.
520                  The following is a sample:  JOSEPH*START.someelementname1
530                      @RUN userID,account #,projectID, paramenters
540                      @SYM PRINT$,,line printer #
550                      @ASG,A JOSEPH*FRANCIS
560                      @ASG,A JOSEPH*DATA
570                      @ASG,A JOSEPH*RUNDATA
580                      @USE 7,JOSEPH*RUNDATA.
```

(Consult program listing for detail of subroutines.)

```
                    @XQT JOSEPH*FRANCIS.CUSHEQ/DOUBLE
                    @ADD JOSEPH*DATA.someelementname2
                    @COPY.I 7..JOSEPH*DATA.someelementname3
                    @FIN

          NOTE:  someelementname# means a DIFFERENT name must
                 be used each time the program is run otherwise
                 the last run will be wiped out!!
       5.  Free all files involved and do not access them between
           issuing the START command illustrated in step 6. and the
           time that the job actually runs.
       6.  Start the run:
           ->PXQT START JOSEPH*START.someelementname1

II.  To Plot - You MUST be on a terminal that supports graphics!
          1.  Assign a temporary file
              ->PXQT ASG,T 7.
          2.  Copy the output data into 7.
              ->PXQT COPY.I JOSEPH*DATA.someelementname3.7.
          3.  You will need the following information for step 4:
              -The unit number to read data from.
               the one you assigned in 1.
              -The number of elements in the array.
               If you don't know the number.
               type OLO 7. and then type LENGTH.
               Subtract 11 from the answer to get the
               number of data points.
              -The format the data was written with.  We had
               originally used 2020.8. then switched to
               2D23.11 to compare with the Dutch results.
               If you don't know the format,
               type OLO 7.. (if you haven't already done so)
               then type PRINT +10
               Count the number of digits after the decimal in
               the last column of numbers.  It should be 8 or 11,
               so use 2020.8 or 2D23.11. as appropriate.
          4.  Execute the program
              >XQT JOSEPH*FRANCIS.SPREAD/DOUBLE
              The program will prompt you for the information.
              and ask questions about your plotting choices.

            When it is done plotting, it will pause for you.
            When you have finished staring at it, copying data
            from it, and/or making a hard copy. THEN AND ONLY
            THEN hit return and it will prompt you for more
            graphs.

@OFFSEND.SZN
```

APPENDIX B CIRCUIT ALGEBRA

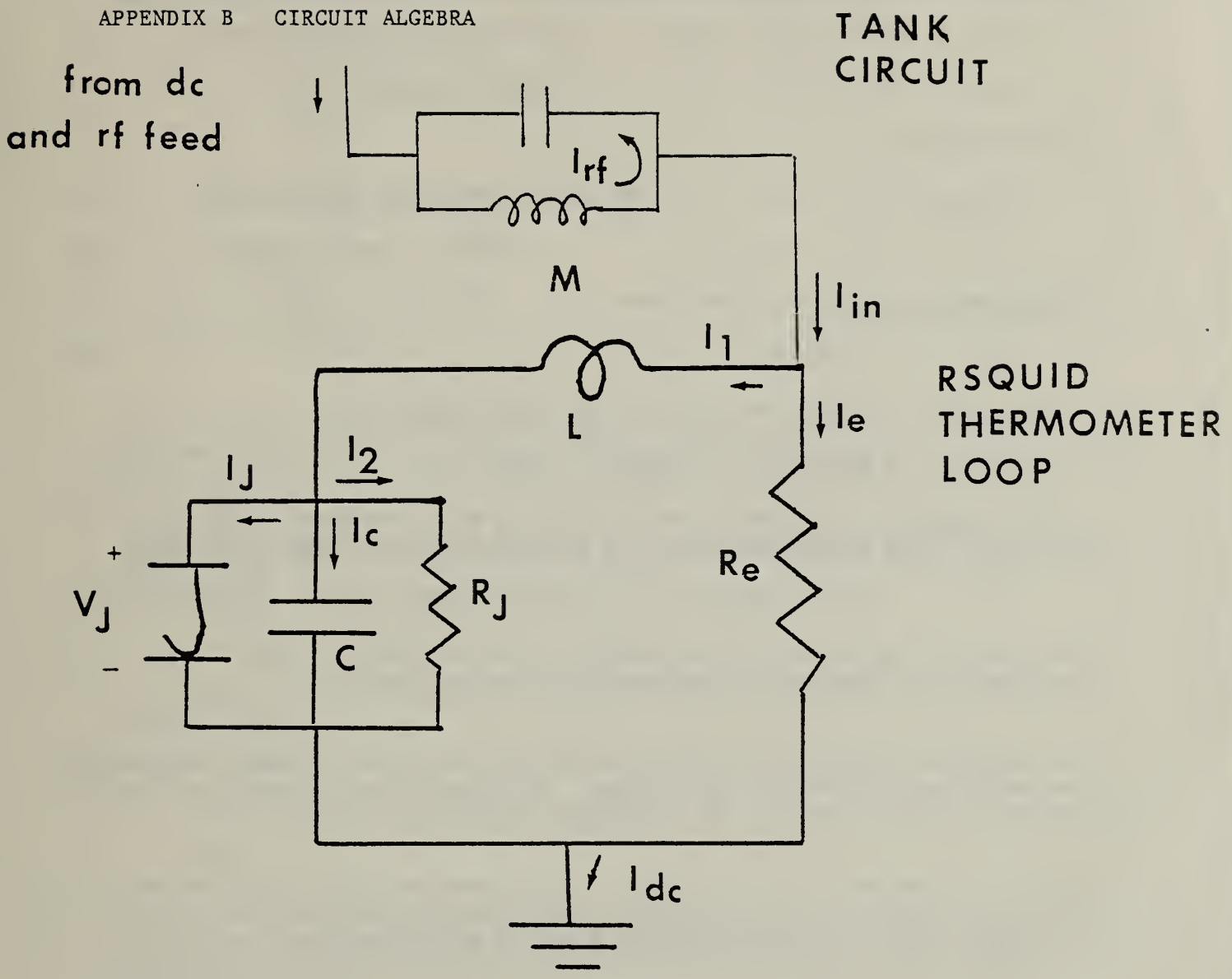

Point Contact

C (parasitic) capacitance of this

R_J Resistance associated with the quasiparticle conduction

L Single coupling loop (inductance at nanohenry level)

R_e Shunt Resistor, typically of silicon bronze

Josephson relations in the point-contact branch (an active device)

$$V_J = 1/2\pi \cdot h/2e \cdot d\phi/dt \qquad \text{instantaneous Josephson emf} \qquad (1a)$$

$$I_{sc} = I_c \sin \phi(t) = I_J \qquad \text{tunneling supercurrent} \qquad (1b)$$

Current division:

$$I_{in} = I_1 + I_e \qquad \text{at input terminal to RSQUID loop} \qquad (2)$$

$$I_1 = I_J + I_c + I_2 \qquad \text{at input to point contact} \qquad (3)$$

Displacement current in capacitance

$$I_c = C \cdot dV_J/dt \qquad (4)$$

Voltage closure around the emf's of the main RSQUID loop

$$V_J = M\, dI_{rf}/dt + L\, dI_1/dt + R_e I_e \qquad (5)$$

We assume that the tank circuit functions as a constant-current rf source, and that the dc bias feed comes from a constant-current source, so that

$$I_{in} = \eta I_{rf} + I_{dc} \qquad \eta < 1 \text{ , where } I_{rf} = i_{rf} \sin \omega t \qquad (6)$$

Here I_{rf} is the rf current resonating in the tank circuit, and η represents the fraction of this which is diverted into I_{in} .

We substitute into (5) and combine these relations into a single equation for the emf's around the main RSQUID loop. With regrouping of terms, we obtain the full equation for ϕ as a function of time.

$$1/2\pi \cdot h/2e \left\{ - L C_J\, d\phi^3/dt^3 + \left[R_e C_J - L/R_J \right] d\phi^2/dt^2 \right.$$

$$\left. + \left[1 + R_e/R_J - Ic\, L \cos \phi \right] d\phi/dt \right\} + R_e I_c \sin \phi$$

$$= R_e I_{dc} + \left[M \omega + \eta R_e \right] i_{rf} \sin \omega t \qquad (7)$$

The third derivative term, and the second term within the second bracket are neglected. We take four new definitions of parameters:

$$\beta \equiv R_e C_J - L/R_J$$

$$\gamma \equiv - I_c L$$

$$\alpha \equiv (R_e I_{dc})/(R_e I_c) = I_{dc} / I_c \qquad \text{dc bias}$$

$$k\omega \equiv \frac{[M + \eta R_e] i_{rf}}{R_e I_c} \qquad \text{rf drive amplitude}$$

and note that there is no loss of generality in assuming γ positive, except that we must recall this reversal of sign when re-interpreting emf's on the inductance L. This achieves the expected positions of the coefficients.

If in addition we scale the frequency ω to the plasma frequency of the RSQUID loop, which is set by the coefficient of the sine term (the product of the critical current I_c and the shunt resistor R_e):

$$2\pi \omega_c = 2e/h \cdot R_e I_c = 1$$

we obtain the greatly simplified general form for the RSJ equation of the RSQUID loop.

$$\beta\ddot{\phi} + (1+\gamma\cos\phi)\dot{\phi} + \sin\phi = \alpha + k\omega \sin\omega t \qquad (8)$$

Here we have tacitly assumed that $R_e/R_J \ll 1$, so that in fact we neglect entirely the quasiparticle tunneling current through the point contact at the very low temperature of the RSQUID thermometer. This enables us to drop the subscript on R_e and to write it as R in the scaling description starting on p. 11.

When, in addition, we assume a positive value of .001 for β, we are implicitly forcing a "smoothing" time constant upon the system response during the short "jump" intervals:

$$\tau_{RC} = R_e C \approx \beta \cdot 2\pi/\omega_c = .21 \text{ microseconds}$$

This detailed circuit model was derived in a slightly different manner by D. van Vechten (private communication, 1980) and has been partially published in references (7), (8), and (9).

NBS-114A (REV. 2-8C)

U.S. DEPT. OF COMM. BIBLIOGRAPHIC DATA SHEET (See instructions)	1. PUBLICATION OR REPORT NO. NBSIR 83-2643	2. Performing Organ. Report No.	3. Publication Date January 1983

4. TITLE AND SUBTITLE

WAVE FORM SIMULATIONS FOR JOSEPHSON JUNCTION CIRCUITS USED FOR NOISE THERMOMETRY

5. AUTHOR(S)

F. Sullivan, D. Kahaner, H. A. Fowler, and J. Knapp-Cordes

6. PERFORMING ORGANIZATION (If joint or other than NBS, see instructions)

NATIONAL BUREAU OF STANDARDS
DEPARTMENT OF COMMERCE
WASHINGTON, D.C. 20234

7. Contract/Grant No.

8. Type of Report & Period Covered

9. SPONSORING ORGANIZATION NAME AND COMPLETE ADDRESS (Street, City, State, ZIP)

N/A

10. SUPPLEMENTARY NOTES

☐ Document describes a computer program; SF-185, FIPS Software Summary, is attached.

11. ABSTRACT (A 200-word or less factual summary of most significant information. If document includes a significant bibliography or literature survey, mention it here)

Solutions to the Resistively Shunted Junction (RSJ) Equation:

$$\beta\ddot{\phi} + (1 + \gamma\cos\phi)\dot{\phi} + \sin\phi = \alpha + k\omega\sin\omega t$$

for small β (= .001) have been approximated using the SDRIVE integration package. Various graphic displays are used to examine the output, including plots of ϕ, $d\phi/dt$, and $\sin\phi$ as functions of time; Poincaré diagrams; and plots of the Lienard coordinate

$$z = \beta\dot{\phi} + \phi + \gamma\sin\phi$$

which has a close connection with the "slow manifold", as a function of ϕ, of $\sin\phi$, and of time. Integration is performed by separation of the second-order equation into a coupled pair of first-order equations, and numerically integrating with respect to time.

Several cases have been examined, for $\gamma < 1$, representing quiet behavior of resistively shunted thermometer oscillator devices. The report is an archive record of program-test data.

A case of "jump"(voltage-spike) oscillator performance for $\gamma = 1.5$ has been simulated in considerable detail, principally as a test of the integrator. Parallel, independent computer results (Sanders and van Veldhuizen, Amsterdam) were available for comparison. This case is of considerable mathematical interest, and values of $|\gamma| > 1$ may also occur in the RSQUID thermometer.

12. KEY WORDS (Six to twelve entries; alphabetical order; capitalize only proper names; and separate key words by semicolons)

Josephson Junction, electronic oscillator, differential equation, numerical integration, Poincaré maps, relaxation oscillator

13. AVAILABILITY

- [X] Unlimited
- [X] For Official Distribution. Do Not Release to NTIS
- [ ] Order From Superintendent of Documents, U.S. Government Printing Office, Washington, D.C. 20402.
- [X] Order From National Technical Information Service (NTIS), Springfield, VA. 22161

14. NO. OF PRINTED PAGES

15. Price